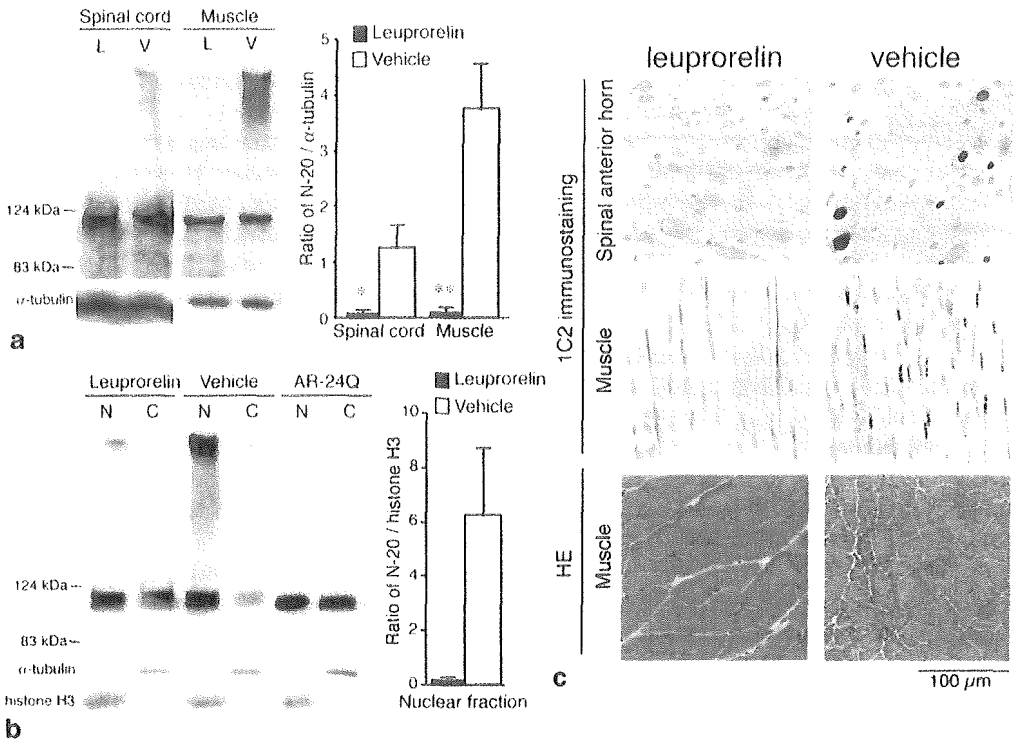

Fig. 3a–c Effects of leuprorelin on mutant AR expression and neuropathology of male AR-97Q mice. **a** Western blot analysis with an anti-AR antibody (N-20) of total homogenates from the spinal cord and muscle of the leuprorelin-treated (*L*) and vehicle-treated (*V*) male AR-97Q mice. Densitometric analysis demonstrated that leuprorelin significantly diminished the amount of mutant AR smearing from the top of the gel. (**P*=0.011, ***P*=0.015). **b** Western blot analysis (with N-20) of the nuclear (*N*) and cytoplasmic (*C*) fractions from muscle tissues of the male mice given leuprorelin (*L*) and vehicle (*V*), and a transgenic mouse carrying an AR with 24 CAG repeats (*AR-24Q*). Smearing mutant AR, which decreased with leuprorelin treatment, was contained in the nuclear fraction. In the densitometric analysis, leuprorelin significantly reduced the amount of smearing mutant AR in the nuclear fraction. (*P*=0.014). **c** Immunohistochemical studies using 1C2 showed marked differences in diffuse nuclear staining and nuclear inclusions between the leuprorelin-treated and vehicle-treated AR-97Q male mice in the spinal anterior horn and the muscle. Hematoxylin and eosin staining of the muscle in the vehicle-treated male mouse revealed apparent grouped atrophy and small angulated fibers, which were not seen in the leuprorelin-treated mice. This figure is reproduced from [53]

SBMA [52, 57]. This may be the reason why flutamide showed no therapeutic effect in our transgenic mouse model of SBMA, and hence is not likely to be a useful therapeutic agent for SBMA.

The castrated or leuprorelin-treated AR-97Q mice showed phenotypes similar to those of the female AR-97Q mice, implying that the motor impairment of SBMA patients can be reduced to the level seen in females. SBMA has been considered an X-linked disease, whereas other polyQ diseases show autosomal dominant inheritance. In fact, female SBMA patients hardly manifest clinical phenotypes, although they possess similar number of CAG repeats in the disease allele as their male siblings with SBMA [24, 25]. Indeed the lower level of mutant AR expression in females due to X-inactivation may cause the escape from phenotypic manifestations, but hormonal interventions in mouse and fly models strongly suggest that low levels of testosterone prevent the nuclear accumulation of the mutant AR, resulting in a lack of phenotypic manifestations in females. This hypothesis is supported by the finding that manifestation of symptoms is minimal, even in females homozygous for SBMA [58]. In another case report, an 85-year-old woman with 38/51 CAG repeats was also asymptomatic [59]. It would appear logical that SBMA is not an X-linked recessive inherited disease, but rather that its phenotype depends on testosterone concentration.

Ligand-dependent modifications of the AR

In addition to nuclear translocation, ligand binding modulates AR function in various ways. These ligand effects are also likely to influence the pathogenesis of SBMA (Fig. 4). Many components of the ubiquitin-proteasome and molecular chaperones are known to co-localize with polyQ-containing NIs [60, 61, 62]. These chaperones and proteasomes facilitate refolding or degradation of the mutant protein, and may play a role in protecting neuronal cells against the toxicity of the expanded polyQ tract [60, 63]. Over-expression of heat shock proteins (HSPs) decreases aggregate formation of mutant ARs and markedly prevents the cell death in a neuronal cell model of SBMA [64]. HSP70 over-expres-

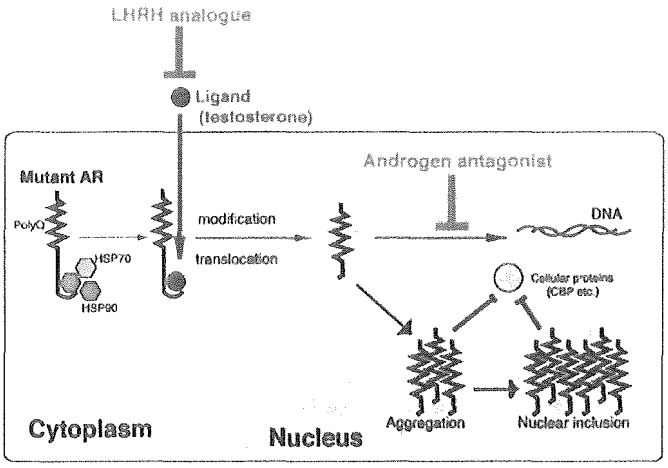

Fig. 4 Hypothetical relationship between the ligand and the mutant AR. In the absence of ligand, the mutant AR is confined to a multi-heteromeric inactive complex with heat shock proteins (*HSP*) in the cell cytoplasm. Ligand-binding facilitates its dissociation from this complex and translocation into the nucleus. Ligand also induces AR modifications such as conformational change, phosphorylation and proteolytic cleavage. In the nucleus, the mutant AR aggregates in a fashion partially dependent on transglutaminase activity, and forms nuclear inclusions as a consequence. The function of critical cellular proteins such as CREB-binding protein is inhibited by mutant the AR, resulting in transcriptional dysregulation. On the other hand, the decreased transactivation function of the mutant AR may contribute to the androgen insensitivity and neurodegeneration in SBMA. LHRH agonist, but not androgen antagonist, inhibits nuclear accumulation of mutant AR, resulting in the improvement of SBMA phenotypes in model mice. This figure is modified from [103]

sion enhances both the solubility and the degradation of mutant ARs in vitro [65]. These protective effects of the HSPs have also been reported in a wide range of polyQ disease models [60, 66, 67, 68]. Over-expression of the inducible form of human HSP70 markedly ameliorated the symptomatic and histopathological phenotypes in our transgenic mouse model, and this amelioration was correlated with the reduction in the amount of nuclear-localized mutant AR protein [69]. It should be noted that the soluble form of the mutant AR was also significantly decreased by HSP70 over-expression, suggesting that the degradation of the mutant AR may have been accelerated by over-expression of HSP70. Without ligand stimulation, the AR is associated with HSP70 and HSP90, and exists as an inactivated complex in the cell cytoplasm. Once ligand binds to the AR, the receptor is released from this complex and translocates into the nucleus. Ligand-dependent dissociation from HSPs is likely to enhance the toxic properties of mutant ARs, and thus contributes to the pathogenesis of SBMA. Supporting this hypothesis, ligand induces mutant AR aggregation even in the cytoplasm in a cell model of SBMA [70].

Proteolytic cleavage or truncation of mutant proteins appears to be of importance for the pathogenesis of polyQ diseases. In transgenic mouse models of HD and those of Machado-Joseph disease, or SCA3, the truncated protein has a particularly pronounced effect on the disease manifestation [71, 72]. NIs are detected by antibodies against an N-terminal epitope, but not by antibodies against a C-terminal epitope in SBMA [41, 42] as well as in other polyQ diseases [73]. These findings suggest that truncated polyQ-containing proteins confer the toxicity in polyQ diseases. It should be noted that a truncated mutant AR is more toxic than the full-length AR in a SBMA cell model [74]. Additionally, in vitro translated full-length AR protein with an expanded polyQ tract is cleaved by caspase-3, liberating a polyQ-containing fragment, and the susceptibility to cleavage is polyQ repeat length-dependent [75]. Thus, cleavage of polyQ-containing proteins is likely to contribute to the toxicity of polyQ tracts. Testosterone induces a conformation change in the AR, resulting in an altered propensity for proteolytic cleavage. It should be noted that the AR antagonist flutamide exerts the same effect as testosterone on mutant AR cleavage in a fly model of SBMA [52]. The activity of caspase-3 is also enhanced by phosphorylation of the AR, resulting in enhanced cytotoxicity of the polyQ tract [76]. Phosphorylation of the mutant protein is required for polyQ-induced neurodegeneration in both SCA-1 cell and fly models of SMBA [77, 78]. Phosphorylation of the AR is known to be modulated by ligand [79], indicating that ligand-dependent phosphorylation of mutant ARs would appear to contribute to the pathogenesis of SBMA. The exact role of AR phosphorylation in SBMA should be elucidated.

Transglutaminase has also been hypothesized to enhance polyQ toxicity [80, 81]. Mutant proteins with an expanded polyQ tract are preferential substrates for transglutaminase, which catalyzes glutamyl-lysine cross-linking, resulting in the formation of proteolysis-resistant aggregates. The AR is a substrate for transglutaminase, which induces cross-linking of mutant ARs and alters their epitope properties in vitro [82]. Transglutaminase bond formation is found in the tissues of SBMA transgenic mice, suggesting its involvement in pathogenesis. Mutant AR and transglutaminase both induce a perturbation of proteasomal function in the presence of testosterone. The degradation of the AR protein is markedly retarded by its ligands [83]. Taken together, these findings suggest that the disruption of the proteasome, which has been implicated in the pathogenesis of SBMA and other polyQ diseases [84, 85], also appears to be ligand-dependent in SBMA.

As in other polyQ diseases, a toxic gain-of-function mutation has been implicated in the pathophysiology of SBMA. Although the expansion of its polyQ tract mildly suppresses the transcriptional activities of the AR [86, 87], motor impairment has never been observed in severe testicular feminization patients lacking AR function [88] or in AR knockout mice [89]. A transgenic mouse model carrying 239 CAG repeat driven by the human AR promoter demonstrated motor impairment, suggesting that the presence of a polyQ tract is sufficient to induce the pathogenic process of SBMA [62]. Thus, the neurological impairment in SBMA is not to be attributed to the loss of AR function, a reason why testosterone shows transient

and insufficient effects when used as a therapeutic agent for SBMA [28, 29, 30]. However, recent data have demonstrated that loss of normal protein function also plays a role in the neurodegeneration in polyQ diseases. As for the AR, there are several lines of evidence in favor of ligand-induced neuroprotective effects. Exogenous administration of testosterone immediately after nerve injury impacts positively on functional recovery through actions mediated by AR [90, 91]. In a cell culture model, a mutant AR with 24 CAG repeats shows trophic effects upon ligand treatment, whereas an AR with 65 CAG repeats does not demonstrate any neuroprotection [92]. Ligand effects on AR function should be further studied using animal models of SBMA.

Therapeutic perspectives in SBMA and other polyQ diseases

As mentioned above, our recent study indicated that leuprorelin exerts a therapeutic effect in the SBMA transgenic mouse model. This approach can easily be applied to human SBMA therapy, because this drug has extensively been used for medical castration in the therapy of prostate cancer [93]. When we move on to clinical trials of hormonal therapy, it is necessary to determine clinical and laboratory markers reflecting the disease activity. Muscle strength, muscle volume and bulbar function would be reasonable parameters, although they must be quantified. Early symptoms, including hand tremor, muscle cramps or mild weakness could be the key for treatment initiation, only if the patients have no wish to have children. Although no specific ligand for the mutant protein has been revealed in other polyQ diseases, the striking therapeutic effects of leuprorelin in our SBMA mice further suggest that patients with other forms of polyQ disease can be treated by preventing the nuclear translocation of the mutant protein in question. Our studies with transgenic mice also indicate that overexpression or activation of HSP would be of therapeutic benefit in polyQ diseases. Medical approaches to enhance HSP function should be further investigated in vivo.

Besides these strategies, various molecular mechanisms are likely to be the therapeutic targets in polyQ diseases. The function of transcription factors such as CREB-binding protein (CBP) are inhibited through protein-protein interaction in mouse models and patients with polyQ diseases [94, 95]. HDAC inhibitors, which restore histone acetylation by CBP, improve transcriptional activity and ameliorate polyQ-induced neurodegeneration in a cell model of SBMA [96] as well as in a fly model of HD [97], although this is of limited therapeutic benefit in a mouse model of HD due to toxicity [98]. Protein aggregation has been shown to render polyQ-containing proteins toxic in numerous cell models of SBMA and other polyQ diseases [99, 100]. The azo-dye Congo Red inhibits oligomerization of mutant huntingtin, and ameliorates motor function and survival of in a transgenic mouse model of HD [101]. Cystamine, a transglutaminase inhibitor, has been shown to mitigate polyQ toxicity in a cell model of SBMA [82] as well as in a HD mouse model [102]. Clinical applications of these therapeutic approaches are awaited.

The ideal treatment for polyQ diseases appears to be a combination of these and other therapeutic strategies, since each approach has adverse effect and long-term treatment is unavoidable. Elucidation ofpathophysiology, high-throughput drug screening and intensive clinical trials are necessary for establishing effective therapeutic strategies.

Acknowledgements This work was supported by a Center-of-Excellence (COE) grant from the Ministry of Education, Culture, Sports, Science and Technology, Japan, grants from the Ministry of Health, Labour and Welfare, Japan, by a grant from the Naito Foundation, and by a grant from the Kanae Foundation.

References

1. Kawahara H (1897) A family with progressive bulbar palsy. Aichi Med J 16:3–4
2. Takahashi A (2001) Hiroshi Kawahara (1858–1918). J Neurol 248:241–242
3. Takikawa K (1953) A pedigree of progressive bulbar paralysis appearing with sex-linked recessive inheritance. Jpn J Hum Genet 28:116–125
4. Kurland LT (1957) Epidemiologic investigations of amyotrophic lateral sclerosis. III. A genetic interpretation of incidence and geographic distribution. Mayo Clin Proc 32:449–462
5. Magee KR (1960) Familial progressive bulbar-spinal muscular atrophy. Neurology 10:295–305
6. Tsukagoshi H, Nakanishi T, Kondo K, Tsubaki T (1965) Hereditary proximal neurogenic muscular atrophy in adults. Arch Neurol 12:597–603
7. Smith JB, Patel A (1965) Wohlfart-Kugelberg-Welander disease: review of the literature and report of a case. Neurology 15:469–473
8. Gross M (1966) Proximal spinal and muscular atrophy. J Neurol Neurosurg Psychiatry 29:29–34
9. Kennedy WR, Alter M, Sung JH (1968) Progressive proximal spinal and bulbar muscular atrophy of late onset: a sex-linked recessive trait. Neurology 18:671–680
10. La Spada AR, Wilson EM, Lubahn DB, Harding AE, Fischbeck KH (1991) Androgen receptor gene mutations in X-linked spinal and bulbar muscular atrophy. Nature 352:77–79
11. Sobue G, Hashizume Y, Mukai E, Hirayama M, Mitsuma T, Takahashi A (1989) X-linked recessive bulbospinal neuronopathy: a clinicopathological study. Brain 112:209–232
12. Sperfeld AD, Karitzky J, Brummer D, Schreiber H, Haussler J, Ludolph AC, Hanemann CO (2002) X-linked bulbospinal neuropathy: Kennedy disease. Arch Neurol 59:1921–1926
13. Sobue G, Adachi H, Katsuno M (2003) Spinal and bulbar muscular atrophy (SBMA). In: Dickinson D (ed) Neurodegeneration: the molecular pathology of dementia and movement disorders. INS Neuropathology, Basel, pp 275–279
14. Hausmanowa-Petrusewicz I, Borkowska J, Janczewski Z (1983) X-linked adult form of spinal muscular atrophy. J Neurol 229:175–188
15. Arbizu T, Santamaria J, Gomez JM, Quilez A, Serra JP (1983) A family with adult spinal and bulbar muscular atrophy, X-linked inheritance and associated testicular failure. J Neurol Sci 59:371–382
16. Nagashima T, Seko K, Hirose K, Mannen T, Yoshimura S, Arima R, Nagashima K, Morimatsu Y (1988) Familial bulbospinal muscular atrophy associated with testicular atrophy and

sensory neuropathy (Kennedy-Alter-Sung syndrome): autopsy case report of two brothers. J Neurol Sci 87:141–152
17. Dejager S, Bry-Gauillard H, Bruckert E, Eymard B, Salachas F, Leguern E, Tardieu S, Chadarevian R, Giral P, Turpin G (2002) A comprehensive endocrine description of Kennedy's disease revealing androgen insensitivity linked to CAG repeat length. J Clin Endocr Metab 87:3893–3901
18. Harding AE, Thomas PK, Baraitser M, Bradbury PG, Morgan-Hughes JA, Ponsford JR (1982) X-linked recessive bulbospinal neuronopathy: a report of ten cases. J Neurol Neurosurg Psychiatry 45:1012–1019
19. Kachi T, Sobue G, Sobue I (1992) Central motor and sensory conduction in X-linked recessive bulbospinal neuronopathy. J Neurol Neurosurg Psychiatry 55:394–397
20. Warner CL, Servidei S, Lange DJ, Miller E, Lovelace RE, Rowland LP (1990) X-linked spinal muscular atrophy (Kennedy's syndrome): a kindred with hypobetalipoproteinemia. Arch Neurol 47:1117–1120
21. Fischbeck KH (1997) Kennedy disease. J Inherit Metab Dis 20:152–158
22. Parboosingh JS, Figlewicz DA, Krizus A, Meininger V, Azad NA, Newman DS, Rouleau GA (1997) Spinobulbar muscular atrophy can mimic ALS: the importance of genetic testing in male patients with atypical ALS. Neurology 49:568–572
23. Udd B, Juvonen V, Hakamies L, Nieminen A, Wallgren-Pettersson C, Cederquist K, Savontaus M-L (1998) High prevalence of Kennedy's disease in western Finland: is the syndrome underdiagnosed? Acta Neurol Scand 98:128–133
24. Sobue G, Doyu M, Kachi T, Yasuda T, Mukai E, Kumagai T, Mitsuma T (1993) Subclinical phenotypic expressions in heterozygous females of X-linked recessive bulbospinal neuronopathy. J Neurol Sci 117:74–78
25. Mariotti C, Castellotti B, Pareyson D, Testa D, Eoli M, Antozzi C, Silani V, Marconi R, Tezzon F, Siciliano G, Marchini C, Gellera C, Donato SD (2000) Phenotypic manifestations associated with CAG-repeat expansion in the androgen receptor gene in male patients and heterozygous females: a clinical and molecular study of 30 families. Neuromuscul Disord 10:391–397
26. Sobue G, Matsuoka Y, Mukai E, Takayanagi T, Sobue I, Hashizume Y (1981) Spinal and cranial motor nerve roots in amyotrophic lateral sclerosis and X-linked recessive bulbospinal muscular atrophy: morphometric and teased-fiber studies. Acta Neuropathol 55:227–235
27. Li M, Sobue G, Doyu M, Mukai E, Hashizume Y, Mitsuma T (1995) Primary sensory neurons in X-linked recessive bulbospinal neuropathy: histopathology and androgen receptor gene expression. Muscle Nerve 18:301–308
28. Danek A, Witt TN, Mann K, Schweikert HU, Romalo G, La Spada AR, Fischbeck KH (1994) Decrease in androgen binding and effect of androgen treatment in a case of X-linked bulbospinal neuronopathy. Clin Investig 72:892–897
29. Goldenberg JN, Bradley WG (1996) Testosterone therapy and the pathogenesis of Kennedy's disease (X-linked bulbospinal muscular atrophy). J Neurol Sci 135:158–161
30. Neuschmid-Kaspar F, Gast A, Peterziel H, Schneikert J, Muigg A, Ransmayr G, Klocker H, Bartsch G, Cato AC (1996) CAG-repeat expansion in androgen receptor in Kennedy's disease is not a loss of function mutation. Mol Cell Endocrinol 117:149–156
31. Tanaka F, Doyu M, Ito Y, Matsumoto M, Mitsuma T, Abe K, Aoki M, Itoyama Y, Fischbeck KH, Sobue G (1996) Founder effect in spinal and bulbar muscular atrophy (SBMA). Hum Mol Genet 5:1253–1257
32. Lund A, Udd B, Juvonen V, Andersen PM, Cederquist K, Davis M, Gellera C, Kolmel C, Ronnevi L-O, Sperfeld A-D, Sorensen S-A, Tranebjaerg L, van Maldergem L, Watanabe M, Weber M, Yeung L, Savontaus M-L (2001) Multiple founder effects in spinal and bulbar muscular atrophy (SBMA, Kennedy disease) around the world. Eur J Hum Genet 9:431–436
33. Zoghbi HY, Orr HT (2000) Glutamine repeats and neurodegeneration. Annu Rev Neurosci 23:217–247
34. Ross CA (2002) Polyglutamine pathogenesis: emergence of unifying mechanisms for Huntington's disease and related disorders. Neuron 35:819–822
35. Taylor JP, Hardy J, Fischbeck KH (2002) Toxic proteins in neurodegenerative disease. Science 296:1991–1995
36. Doyu M, Sobue G, Mukai E, Kachi T, Yasuda T, Mitsuma T, Takahashi A (1992) Severity of X-linked recessive bulbospinal neuronopathy correlates with size of the tandem CAG repeat in androgen receptor gene. Ann Neurol 32:707–710
37. Tanaka F, Reeves MF, Ito Y, Matsumoto M, Li M, Miwa S, Inukai A, Yamamoto M, Doyu M, Yoshida M, Hashizume Y, Terao S, Mitsuma T, Sobue G (1999) Tissue-specific somatic mosaicism in spinal and bulbar muscular atrophy is dependent on CAG-repeat length and androgen receptor gene expression level. Am J Hum Genet 65:966–973
38. Doyu M, Sobue G, Kimata K, Yamamoto K, Mitsuma T (1994) Androgen receptor mRNAs with increased size of tandem CAG repeats are widely expressed in the neural and nonneural tissues of X-linked recessive bulbospinal neuronopathy. J Neurol Sci 127:43–47
39. La Spada AR, Roling DB, Harding AE, Warner CL, Spiegel R, Hausmanowa-Petrusewicz I, Yee WC, Fischbeck KH (1992) Meiotic stability and genotype-phenotype correlation of the trinucleotide repeat in X-linked spinal and bulbar muscular atrophy. Nat Genet 2:301–304
40. Margolis RL, Ross CA (2002) Expansion explosion: new clues to the pathogenesis of repeat expansion neurodegenerative diseases. Trends Mol Med 7:479–482
41. Li M, Miwa S, Kobayashi Y, Merry DE, Yamamoto M, Tanaka F, Doyu M, Hashizume Y, Fischbeck KH, Sobue G (1998) Nuclear inclusions of the androgen receptor protein in spinal and bulbar muscular atrophy. Ann Neurol 44:249–254
42. Li M, Nakagomi Y, Kobayashi Y, Merry DE, Tanaka F, Doyu M, Mitsuma T, Hashizume Y, Fischbeck KH, Sobue G (1998) Non-neural nuclear inclusions of androgen receptor protein in spinal and bulbar muscular atrophy. Am J Pathol 153:695–701
43. Klement IA, Skinner PJ, Kaytor MD, Yi H, Hersch SM, Clark HB, Zoghbi HY, Orr HT (1998) Ataxin-1 nuclear localization and aggregation: role in polyglutamine-induced disease in SCA1 transgenic mice. Cell 95:41–53
44. Steffan JS, Kazantsev A, Spasic-Boskovic O, Greenwald M, Zhu YZ, Gohler H, Wanker EE, Bates GP, Housman DE, Thompson LM (2000) The Huntington's disease protein interacts with p53 and CREB-binding protein and represses transcription. Proc Natl Acad Sci USA 97:6763–6768
45. Nucifora FC Jr, Sasaki M, Peters MF, Huang H, Cooper JK, Yamada M, Takahashi H, Tsuji S, Troncoso J, Dawson VL, Dawson TM, Ross CA (2001) Interference by huntingtin and atrophin-1 with CBP-mediated transcription leading to cellular toxicity. Science 291:2423–2428
46. Zhou ZX, Lane MV, Kemppainen JA, French FS, Wilson EM (1995) Specificity of ligand-dependent androgen receptor stabilization: receptor domain interactions influence ligand dissociation and receptor stability. Mol Endocrinol 9:208–218
47. Katsuno M, Adachi H, Kume A, Li M, Nakagomi Y, Niwa H, Sang C, Kobayashi Y, Doyu M, Sobue G (2002) Testosterone reduction prevents phenotypic expression in a transgenic mouse model of spinal and bulbar muscular atrophy. Neuron 35:843–854
48. McManamny P, Chy HS, Finkelstein DI, Craythorn RG, Crack PJ, Kola I, Cheema SS, Horne MK, Wreford NG, O'Bryan MK, De Kretser DM, Morrison JR (2002) A mouse model of spinal and bulbar muscular atrophy. Hum Mol Genet 11:2103–2111
49. Saudou F, Finkbeiner S, Devys D, Greenberg ME (1998) Huntingtin acts in the nucleus to induce apoptosis but death does not correlate with the formation of intranuclear inclusions. Cell 95:55–66

50. Peters MF, Nucifora FC Jr, Kushi J, Seaman HC, Cooper JK, Herring WJ, Dawson VL, Dawson TM, Ross CA (1999) Nuclear targeting of mutant Huntingtin increases toxicity. Mol Cell Neurosci 14:121–128
51. Jackson WS, Tallaksen-Greene SJ, Albin RL, Detloff PJ (2003) Nucleocytoplasmic transport signals affect the age at onset of abnormalities in knock-in mice expressing polyglutamine within an ectopic protein context. Hum Mol Genet 12:1621–1629
52. Takeyama K, Ito S, Yamamoto A, Tanimoto H, Furutani T, Kanuka H, Miura M, Tabata T, Kato S (2002) Androgen-dependent neurodegeneration by polyglutamine-expanded human androgen receptor in *Drosophila*. Neuron 35:855–864
53. Katsuno M, Adachi H, Doyu M, Minamiyama M, Sang C, Kobayashi Y, Inukai A, Sobue G (2003) Leuprorelin rescues polyglutamine-dependent phenotypes in a transgenic mouse model of spinal and bulbar muscular atrophy. Nat Med 9:768–773
54. Yamamoto A, Lucas JJ, Hen R (2000) Reversal of neuropathology and motor dysfunction in a conditional model of Huntington's disease. Cell 101:57–66
55. Lu S, Simon NG, Wang Y, Hu S (1999) Neural androgen receptor regulation: effects of androgen and antiandrogen. J Neurobiol 41:505–512
56. Tomura A, Goto K, Morinaga H, Nomura M, Okabe T, Yanase T, Takayanagi R, Nawata H (2001) The subnuclear three-dimensional image analysis of androgen receptor fused to green fluorescence protein. J Biol Chem 276:28395–28401
57. Walcott JL, Merry DE (2002) Ligand promotes intranuclear inclusions in a novel cell model of spinal and bulbar muscular atrophy. J Biol Chem 277:50855–50859
58. Schmidt BJ, Greenberg CR, Allingham-Hawkins DJ, Spriggs EL (2002) Expression of X-linked bulbospinal muscular atrophy (Kennedy disease) in two homozygous women. Neurology 59:770–772
59. Kuhlenbaumer G, Kress W, Ringelstein EB, Stogbauer F (2001) Thirty-seven CAG repeats in the androgen receptor gene in two healthy individuals. J Neurol 248:23–26
60. Cummings CJ, Mancini MA, Antalffy B, DeFranco DB, Orr HT, Zoghbi HY (1998) Chaperone suppression of aggregation and altered subcellular proteasome localization imply protein misfolding in SCA1. Nat Genet 19:148–154
61. Stenoien DL, Cummings CJ, Adams HP, Mancini MG, Patel K, DeMartino GN, Marcelli M, Weigel NL, Mancini MA (1999) Polyglutamine-expanded androgen receptors form aggregates that sequester heat shock proteins, proteasome components and SRC-1, and are suppressed by the HDJ-2 chaperone. Hum Mol Genet 8:731–741
62. Adachi H, Kume A, Li M, Nakagomi Y, Niwa H, Do J, Sang C, Kobayashi Y, Doyu M, Sobue G (2001) Transgenic mice with an expanded CAG repeat controlled by the human AR promoter show polyglutamine nuclear inclusions and neuronal dysfunction without neuronal cell death. Hum Mol Genet 10:1039–1048
63. Kobayashi Y, Sobue G (2001) Protective effect of chaperones on polyglutamine diseases. Brain Res Bull 56:165–168
64. Kobayashi Y, Kume A, Li M, Doyu M, Hata M, Ohtsuka K, Sobue G (2000) Chaperones Hsp70 and Hsp40 suppress aggregate formation and apoptosis in cultured neuronal cells expressing truncated androgen receptor protein with expanded polyglutamine tract. J Biol Chem 275:8772–8778
65. Bailey CK, Andriola IF, Kampinga HH, Merry DE (2002) Molecular chaperones enhance the degradation of expanded polyglutamine repeat androgen receptor in a cellular model of spinal and bulbar muscular atrophy. Hum Mol Genet 11:515–523
66. Warrick JM, Chan HY, Gray-Board GL, Chai Y, Paulson HL, Bonini NM (1999) Suppression of polyglutamine-mediated neurodegeneration in Drosophila by the molecular chaperone HSP70. Nat Genet 23:425–458
67. Carmichael J, Chatellier J, Woolfson A, Milstein C, Fersht AR, Rubinsztein DC (2000) Bacterial and yeast chaperones reduce both aggregate formation and cell death in mammalian cell models of Huntington's disease. Proc Natl Acad Sci USA 97:9701–9705
68. Cummings CJ, Sun Y, Opal P, Antalffy B, Mestril R, Orr HT, Dillmann WH, Zoghbi HY (2001) Over-expression of inducible HSP70 chaperone suppresses neuropathology and improves motor function in SCA1 mice. Hum Mol Genet 10:1511–1518
69. Adachi H, Katsuno M, Minamiyama M, Sang C, Pagoulatos G, Angelidis C, Kusakabe M, Yoshiki A, Kobayashi Y, Doyu M, Sobue G (2003) Heat shock protein 70 chaperone overexpression ameliorates phenotypes of the spinal and bulbar muscular atrophy transgenic mouse model by reducing nuclear-localized mutant androgen receptor protein. J Neurosci 23:2203–2211
70. Darrington RS, Butler R, Leigh PN, McPhaul MJ, Gallo JM (2002) Ligand-dependent aggregation of polyglutamine-expanded androgen receptor in neuronal cells. Neuroreport 13:2117–2120
71. Mangiarini L, Sathasivam K, Seller M, Cozens B, Harper A, Hetherington C, Lawton M, Trottier Y, Lehrach H, Davies SW, Bates GP (1996) Exon 1 of the HD gene with an expanded CAG repeat is sufficient to cause a progressive neurological phenotype in transgenic mice. Cell 87:493–506
72. Ikeda H, Yamaguchi M, Sugai S, Aze Y, Narumiya S, Kakizuka A (1996) Expanded polyglutamine in the Machado-Joseph disease protein induces cell death in vitro and in vivo. Nat Genet 13:196–202
73. DiFiglia M, Sapp E, Chase KO, Davies SW, Bates GP, Vonsattel JP, Aronin N (1997) Aggregation of huntingtin in neuronal intranuclear inclusions and dystrophic neurites in the brain. Science 277:1990–1993
74. Merry DE, Kobayashi Y, Bailey CK, Taye AA, Fischbeck KH (1998) Cleavage, aggregation and toxicity of the expanded androgen receptor in spinal and bulbar muscular atrophy. Hum Mol Genet 7:693–701
75. Kobayashi Y, Miwa S, Merry DE, Kume A, Mei L, Doyu M, Sobue G (1998) Caspase-3 cleaves the expanded androgen receptor protein of spinal and bulbar muscular atrophy in a polyglutamine repeat length-dependent manner. Biochem Biophys Res Commun 252:145–150
76. LaFevre-Bernt MA, Ellerby LM (2003) Kennedy's disease: phosphorylation of the polyQ-expanded form of androgen receptor regulates its cleavage by caspase-3 and enhances cell death. J Biol Chem 278:34918–34924
77. Emamian ES, Kaytor MD, Duvick LA, Zu T, Tousey SK, Zoghbi HY, Clark HB, Orr HT (2003) Serine 776 of ataxin-1 is critical for polyglutamine-induced disease in SCA1 transgenic mice. Neuron 38:375–387
78. Chen HK, Fernandez-Funez P, Acevedo SF, Lam YC, Kaytor MD, Fernandez MH, Aitken A, Skoulakis EM, Orr HT, Botas J, Zoghbi HY (2003) Interaction of Akt-phosphorylated ataxin-1 with 14-3-3 mediates neurodegeneration in spinocerebellar ataxia type 1. Cell 113:457–468
79. van Laar JH, Berrevoets CA, Trapman J, Zegers ND, Brinkmann AO (1991) Hormone-dependent androgen receptor phosphorylation is accompanied by receptor transformation in human lymph node carcinoma of the prostate cells. J Biol Chem 266:3734–3738
80. Igarashi S, Koide R, Shimohata T, Yamada M, Hayashi Y, Takano H, Date H, Oyake M, Sato T, Sato A, Egawa S, Ikeuchi T, Tanaka H, Nakano R, Tanaka K, Hozumi I, Inuzuka T, Takahashi H, Tsuji S (1998) Suppression of aggregate formation and apoptosis by transglutaminase inhibitors in cells expressing truncated DRPLA protein with an expanded polyglutamine stretch. Nat Genet 18:111–117
81. Karpuj MV, Garren H, Slunt H, Price DL, Gusella J, Becher MW, Steinman L (1999) Transglutaminase aggregates huntingtin into nonamyloidogenic polymers, and its enzymatic activity increases in Huntington's disease brain nuclei. Proc Natl Acad Sci USA 96:7388–7393

82. Mandrusiak LM, Beitel LK, Wang X, Scanlon TC, Chevalier-Larsen E, Merry DE, Trifiro MA (2003) Transglutaminase potentiates ligand-dependent proteasome dysfunction induced by polyglutamine-expanded androgen receptor. Hum Mol Genet 12:1497–1506
83. Kemppainen JA, Lane MV, Sar M, Wilson EM (1992) Androgen receptor phosphorylation, turnover, nuclear transport, and transcriptional activation. Specificity for steroids and antihormones. J Biol Chem 267:968–974
84. Chan HY, Warrick JM, Andriola I, Merry D, Bonini NM (2002) Genetic modulation of polyglutamine toxicity by protein conjugation pathways in *Drosophila*. Hum Mol Genet 11:2895–2904
85. Tobin AJ, Signer ER (2000) Huntington's disease: the challenge for cell biologists. Trends Cell Biol 10:531–536
86. Mhatre AN, Trifiro MA, Kaufman M, Kazemi-Esfarjani P, Figlewicz D, Rouleau G, Pinsky L (1993) Reduced transcriptional regulatory competence of the androgen receptor in X-linked spinal and bulbar muscular atrophy. Nat Genet 5:184–188
87. Brooks BP, Paulson HL, Merry DE, Salazar-Grueso EF, Brinkmann AO, Wilson EM, Fischbeck KH (1997) Characterization of an expanded glutamine repeat androgen receptor in a neuronal cell culture system. Neurobiol Dis 3:313–323
88. Gottlieb B, Pinsky L, Beitel LK, Trifiro M (1999) Androgen insensitivity. Am J Med Genet 89:210–217
89. Yeh S, Tsai MY, Xu Q, Mu XM, Lardy H, Huang KE, Lin H, Yeh SD, Altuwaijri S, Zhou X, Xing L, Boyce BF, Hung MC, Zhang S, Gan L, Chang C, Hung MC (2002) Generation and characterization of androgen receptor knockout (ARKO) mice: an in vivo model for the study of androgen functions in selective tissues. Proc Natl Acad Sci USA 99:13498–13503
90. Brooks BP, Merry DE, Paulson HL, Lieberman AP, Kolson DL, Fischbeck KH (1998) A cell culture model for androgen effects in motor neurons. J Neurochem 70:1054–1060
91. Jones KJ, Brown TJ, Damaser M (2001) Neuroprotective effects of gonadal steroids on regenerating peripheral motoneurons. Brain Res Rev 37:372–382
92. Lieberman AP, Harmison G, Strand AD, Olson JM, Fischbeck KH (2002) Altered transcriptional regulation in cells expressing the expanded polyglutamine androgen receptor. Hum Mol Genet 11:1967–1976
93. Huggins C, Hodges CV (1941) Studies on prostate cancer. I. The effects of castration, of estrogen and of androgen injection on serum phosphates in metastatic carcinoma of the prostate. Cancer Res 1:293–297
94. McCampbell A, Taylor JP, Taye AA, Robitschek J, Li M, Walcott J, Merry D, Chai Y, Paulson H, Sobue G, Fischbeck KH (2000) CREB-binding protein sequestration by expanded polyglutamine. Hum Mol Genet 9:2197–2202
95. Nucifora FC Jr, Sasaki M, Peters MF, Huang H, Cooper JK, Yamada M, Takahashi H, Tsuji S, Troncoso J, Dawson VL, Dawson TM, Ross CA (2001) Interference by huntingtin and atrophin-1 with CBP-mediated transcription leading to cellular toxicity. Science 291:2423–2428
96. McCampbell A, Taye AA, Whitty L, Penney E, Steffan JS, Fischbeck KH (2001) Histone deacetylase inhibitors reduce polyglutamine toxicity. Proc Natl Acad Sci USA 98:15179–15184
97. Steffan JS, Bodai L, Pallos J, Poelman M, McCampbell A, Apostol BL, Kazantsev A, Schmidt E, Zhu YZ, Greenwald M, Kurokawa R, Housman DE, Jackson GR, Marsh JL, Thompson LM (2001) Histone deacetylase inhibitors arrest polyglutamine-dependent neurodegeneration in *Drosophila*. Nature 413:739–743
98. Hockly E, Richon VM, Woodman B, Smith DL, Zhou X, Rosa E, Sathasivam K, Ghazi-Noori S, Mahal A, Lowden PA, Steffan JS, Marsh JL, Thompson LM, Lewis CM, Marks PA, Bates GP (2003) Suberoylanilide hydroxamic acid, a histone deacetylase inhibitor, ameliorates motor deficits in a mouse model of Huntington's disease. Proc Natl Acad Sci USA 100:2041–2046
99. Heiser V, Scherzinger E, Boeddrich A, Nordhoff E, Lurz R, Schugardt N, Lehrach H, Wanker EE (2000) Inhibition of huntingtin fibrillogenesis by specific antibodies and small molecules: implications for Huntington's disease therapy. Proc Natl Acad Sci USA 97:6739–6744
100. Taylor JP, Tanaka F, Robitschek J, Sandoval CM, Taye A, Markovic-Plese S, Fischbeck KH (2003) Aggresomes protect cells by enhancing the degradation of toxic polyglutamine-containing protein. Hum Mol Genet 12:749–757
101. Sanchez I, Mahlke C, Yuan J (2003) Pivotal role of oligomerization in expanded polyglutamine neurodegenerative disorders. Nature 421:373–379
102. Karpuj MV, Becher MW, Springer JE, Chabas D, Youssef S, Pedotti R, Mitchell D, Steinman L (2002) Prolonged survival and decreased abnormal movements in a transgenic model of Huntington disease, with administration of the transglutaminase inhibitor cystamine. Nat Med 8:143–149
103. Katsuno M, Adachi H, Sobue G (2004) Sweet relief for Huntington disease. Nat Med 10:123–124

Pathology of early- vs late-onset TTR Met30 familial amyloid polyneuropathy

H. Koike, MD, PhD; K. Misu, MD, PhD; M. Sugiura, MD; M. Iijima, MD; K. Mori, MD, PhD; M. Yamamoto, MD, PhD; N. Hattori, MD, PhD; E. Mukai, MD, PhD; Y. Ando, MD, PhD; S. Ikeda, MD, PhD; and G. Sobue, MD, PhD

Abstract—*Background:* Late-onset type I familial amyloid polyneuropathy (FAP TTR Met30) cases unrelated to endemic foci in Japan show clinical features setting them apart from early-onset cases in endemic foci. *Objective:* To compare pathologic features between the early- and late-onset types. *Methods:* Pathologic findings in FAP TTR Met30 with onset before age 50 in relation to endemic foci (11 cases) were compared with those in 11 later-onset cases unrelated to endemic foci. *Results:* Sural nerve biopsy specimens showed predominantly small-fiber loss in early-onset cases; variable fiber size distribution, axonal sprouting, and relatively preserved unmyelinated fibers characterized late-onset cases. Autopsy cases representing both groups showed amyloid deposition throughout the length of nerves and in sympathetic and sensory ganglia, but amounts were greater in early-onset cases. Amyloid deposition and neuronal cell loss were greater in sympathetic than dorsal root ganglia in early-onset cases; the opposite was true in late-onset cases. Size assessment of remaining neurons in these ganglia suggested predominant loss of small neurons in early-onset cases but loss of neurons of all sizes in late-onset cases. Transthyretin-positive, Congo red-negative amorphous material was more conspicuous in nerves from late- than early-onset cases. In extraneural sites, amyloid was more conspicuous in thyroid and kidney from early-onset cases and in heart and hypophysis from late-onset cases. In early-onset cases, cardiac amyloid deposition was prominent in the atrium and subendocardium but was conspicuous throughout the myocardium in late-onset cases. *Conclusion:* The pathology of early- and late-onset FAP TTR Met30 correlated well with differences in clinical findings.

NEUROLOGY 2004;63:129–138

Familial amyloid polyneuropathy type I (transthyretin Met30-associated familial amyloid polyneuropathy; FAP TTR Met30), in which methionine is substituted for valine at position 30 of transthyretin, is the most common type of FAP in Japan as well as in Western countries.[1-6] In Japan, cases have been particularly concentrated in two geographic areas: the village of Ogawa in Nagano Prefecture on the island of Honshu and the city of Arao in Kumamoto Prefecture on the island of Kyushu.[3,4] Although there are exceptions, typical cases of FAP TTR Met30 in these two endemic foci are characterized by early age at onset (second or third decade), a high penetrance rate, marked autonomic dysfunction, selective loss of superficial sensation including nociception and thermal sensation, atrioventricular conduction block requiring pacemaker implantation, steady progression of disease over 10 to 15 years, and presence of anticipation concerning age at onset.[3,4,7-11]

In contrast to these early-onset FAP TTR Met30 cases in endemic foci, we have reported the presence of a late-onset type of FAP TTR Met30 in a wide distribution throughout Japan.[9,10,12] Features of these cases were distinct from those of early-onset cases related to endemic foci. These differences included onset at ages over 50 years, a low penetrance rate, relatively mild autonomic dysfunction, loss of all sensory modalities rather than sensory dissociation, frequent presence of cardiomegaly, extreme male preponderance, and absence of anticipation concerning age at onset.[9,10,12] These geographic and clinical differences were confirmed in a subsequent nationwide survey.[11] Similar geographic and clinical contrasts between early- and late-onset types of FAP TTR Met30 have been reported in Portugal,[1,5,13] although not in the form of a large-scale comparative study.

The reasons for contrasting features in early- and late-onset FAP with the same mutation in the transthyretin gene have not yet been determined. In the current study, we investigated pathologic features of Japanese patients with early- and late-onset FAP TTR Met30, seeking explanations for the clinical differences.

Patients and methods. Pathologic findings were compared between consecutive patients with early- and late-onset FAP TTR Met30 who attended the Nagoya University Graduate School of Medicine for sural nerve biopsy or autopsy from 1989 to 2003. Inclusion criteria for early-onset cases were FAP TTR Met30 with an onset age under 50 years and a relationship to one of the two Japanese endemic foci within the two most recent prior genera-

From the Department of Neurology (Drs. Koike, Misu, Sugiura, Iijima, Mori, Yamamoto, Hattori, and Sobue), Nagoya University Graduate School of Medicine, Department of Neurology (Dr. Mukai), Nagoya National Hospital, Department of Laboratory Medicine (Dr. Ando), Kumamoto University School of Medicine, and Third Department of Medicine (Dr. Ikeda), Shinshu University School of Medicine, Matsumoto, Japan.

Supported by grants from the Ministry of Health, Labor, and Welfare of Japan.

Received October 8, 2003. Accepted in final form February 23, 2004.

Address correspondence and reprint requests to Dr. G. Sobue, Department of Neurology, Nagoya University Graduate School of Medicine, Nagoya 466-8550, Japan; e-mail: sobueg@med.nagoya-u.ac.jp

Table 1 Background and clinical features of early- and late-onset FAP TTR Met30

Case no.	Sex	Age at onset/ death, y	Duration of illness until biopsy, y	Relationship to endemic foci	Family history	Initial symptom	Sensory dissociation	Cardiac involvement		Cause of death
								Cardiomegaly	Pacemaker implantation	
Early-onset group										
1	F	28/35	—	+	+	A	+	−	+	Sudden death
2	F	37/51	—	+	+	A	+	−	+	Pneumonia
3	M	24/41	3	+	+	A	+	−	−	Pneumonia
4	M	35	2.5	+	ND*	W	+	−	−	
5	F	33	6	+	+	P	−	−	+	
6	M	35	3	+	+	P	+	+	−	
7	M	36	2	+	+	A	+	−	−	
8	M	40	1	+	+	P	+	−	−	
9	M	28	1	+	+	P	+	−	−	
10	F	34	2	+	ND*	A	+	−	+	
11	F	41	3	+	+	A	−	−	+	
Late-onset group										
12	M	64/67	2	−	−	P	+	−	−	Lung cancer
13	M	62/68	3	−	−	P	+	+	−	Heart failure
14	M	52/62	3	−	−	P	−	+	−	Heart failure
15	M	67	2	−	+	P	−	−	−	
16	M	77	0.5	−	−	P, HF	−	+	−	
17	M	56	1	−	−	W	−	+	−	
18	M	61	3	−	−	P	−	+	−	
19	M	56	3	−	−	P	−	+	−	
20	M	58	0.6	−	−	P	−	+	−	
21	M	60	1.25	−	−	A	−	+	−	
22	M	61	5	−	−	P, W	−	−	−	

Cardiomegaly was assessed at the time of first referral to the hospital. No patient belonged to the same kindred as another.

* Fathers of Cases 4 and 10 were from Ogawa Village but died of nonneurologic disease when the patients were children. Statistical significance (early-vs late-onset group) was present in the items of sex ($p < 0.05$), age at onset ($p < 0.0001$), relationship to endemic foci ($p < 0.0001$), family history ($p < 0.0001$), sensory dissociation ($p < 0.01$), cardiomegaly ($p < 0.01$), and pacemaker implantation ($p < 0.05$). Statistical analyses were performed using the χ^2 test or the Mann–Whitney U test as appropriate.

FAP = familial amyloid polyneuropathy; + = present; − = absent; A = autonomic symptoms; W = weakness in the lower legs; P = paresthesia in the legs; HF = heart failure; ND = not determined.

tions. For late-onset cases, inclusion criteria were FAP TTR Met30 with an onset age over 50 years and no relationship to the endemic foci within the two most recent prior generations. To confirm the diagnosis of FAP TTR Met30, DNA analyses for mutation of the transthyretin gene were performed in all patients as described previously.[4,14,15] Informed consent was obtained, and all aspects of the study were approved by the Ethics Committee of Nagoya University Graduate School of Medicine.

Of the 22 patients included, 11 were in the early-onset group and the other 11 belonged to the late-onset group (table 1). No patient in the study belonged to the same kindred as another. Age at onset in the early-onset group was 33.9 ± 5.4 years and in the late-onset group 61.3 ± 6.7 years. Duration from onset of neuropathy to sural nerve biopsy was 2.6 ± 1.5 years in the early-onset group and 2.2 ± 1.4 years in the late-onset group (no significant difference). Duration from onset to death in autopsy cases was 12.7 ± 5.1 years for early-onset disease but only 6.3 ± 3.5 years in late-onset cases. Clinical features in the two groups of patients agreed well with previous descriptions.[3,9,11] In the early-onset group, half of the patients initially had autonomic symptoms, and most patients manifested more profound impairment of superficial than deep sensation (i.e., sensory dissociation). Pacemaker implantation was required in five patients, and the apparent cause of death in one case was sudden cardiac arrest. In the late-onset group, on the other hand, most patients initially manifested paresthesias or weakness in the legs rather than autonomic symptoms. Sensory dissociation was infrequent, and most patients manifested cardiac hypertrophy evident by chest radiography or echocardiography as opposed to atrioventricular conduction block in the early-onset group.

Sural nerve biopsy was performed in nine of the early-onset cases and all of the late-onset cases as described previously.[16-19] Specimens were divided into two portions. The first was fixed in 2.5% glutaraldehyde in 0.125 *M* cacodylate buffer (pH 7.4). Most of this part was embedded in epoxy resin for morphometric and ultrastructural study. Density of myelinated fibers was assessed in toluidine blue-stained semithin sections using a computer-assisted image analyzer (Luzex FS; Nikon, Tokyo, Japan); densities of small and large myelinated fibers were calculated as described previously.[17-19] Clusters of two or more small myelinated fibers enclosed by one basement membrane were considered an instance of axonal sprouting.[20-22] For electron microscopic study,

Table 2 Pathologic findings in sural nerve biopsy specimens

Case no.	MF density, no./mm²				Axonal sprouting of MF, no./mm²	UMF density, no./mm²	Segmental de/remyelination, %	Axonal degeneration, %	Amyloid deposition, %
	Large	Small	Total	Small/large					
Early onset									
3	0	0	0	—*	0	0	ND†	ND†	ND
4	13	13	26	—*	0	0	ND†	ND†	7
5	11	22	33	—*	0	216	8	25	1
6	23	0	23	—*	0	212	ND†	ND†	2
7	711	395	1,106	0.56	0	431	5	21	1
8	2,700	1,449	4,149	0.54	9	2,370	10	17	0+
9	2,015	1,515	3,530	0.75	18	3,663	6	26	0+
10	1,090	427	1,517	0.39	6	844	3	9	4
11	1,659	237	1,896	0.14	10	861	ND	ND	0+
Mean ± SD	914 ± 1,018	451 ± 608	1,364 ± 1,583	0.48 ± 0.23	5 ± 7	993 ± 1,305	6.4 ± 2.7	19.6 ± 6.9	
Controls, n = 3	3,495 ± 179	5,172 ± 528	8,666 ± 665	1.48 ± 0.11		30,104 ± 1,115	3.7 ± 5.5	0.4 ± 0.3	
Late onset									
12	79	487	566	6.16	79	2,370	17	20	0+
13	619	527	1,146	0.85	40	7,973	1	37	0
14	329	1,172	1,501	3.56	184	10,990	8	14	0+
15	66	13	79	—*	0	1,293	19	25	1
16	92	250	342	3.30	53	2,155	2	15	0+
17	461	1,831	2,292	3.97	250	7,111	13	27	1
18	0	2,423	2,423	—*	224	4,310	6	19	0
19	132	132	264	1.00	13	2,586	6	24	0+
20	514	355	869	0.69	26	1,795	4	37	0
21	1,304	1,212	2,516	0.93	105	14,438	6	26	0
22	66	277	343	4.20	40	431	ND†	ND†	1
Mean ± SD	333 ± 386	789 ± 776	1,122 ± 925	2.74 ± 1.95	92 ± 88	7,308 ± 5,417	8.2 ± 6.1	24.4 ± 8.0	
Controls, n = 4	2,891 ± 251	4,995 ± 333	7,886 ± 334	1.74 ± 0.22		29,748 ± 3,587	9.5 ± 6.2	1.9 ± 1.9	

Control values for each group were age matched. Statistical significance (early-vs late-onset group) was present in the items of small/large ($p < 0.05$), axonal sprouting of MF ($p < 0.01$), and UMF density ($p < 0.01$). Statistical analyses were performed using the Mann–Whitney *U* test.

* Populations of myelinated fibers were too small to determine the ratio.
† Teased fibers could not be obtained owing to depletion of myelinated fibers.

MF = myelinated fiber; UMF = unmyelinated fiber; ND = not determined; 0+ = <0.5%.

epoxy resin-embedded specimens were cut into ultrathin transverse sections and stained with uranyl acetate and lead citrate. To assess the density of unmyelinated fibers, electron microscopic photographs were taken at a magnification of 4,000× in a random fashion to cover the area of ultrathin sections as described previously.[17,19,21] Density of unmyelinated fibers was estimated from these electron micrographs. The remainder of the glutaraldehyde-fixed sample was processed for teased fiber study, in which microscopic observations were classified according to criteria described previously.[17,18,23,24] The second portion of the specimen was fixed in 10% formalin solution and embedded in paraffin. Sections were cut by routine methods and stained with hematoxylin and eosin, Congo red, the Klüver–Barrera method, and the Masson trichrome method. Seven sural nerve specimens were obtained from subjects with nonneurologic diseases at autopsy and examined in the same manner as age-matched control subjects (three cases for early-onset group, age 39.0 ± 7.8 years; four cases for late-onset group, age 62.3 ± 7.9 years).

Autopsy was performed in three early-onset cases and three late-onset cases. The nervous system including brain, spinal cord, ventral and dorsal roots, dorsal root ganglia from L3 to L5, and sympathetic ganglia was removed, as were the visceral organs. Tissues were fixed in 10% formalin solution, embedded in paraffin, cut, and stained as described for sural nerve specimens. In two of the early-onset and one of the late-onset cases, the median nerve from the axilla to the wrist and the sciatic/tibial nerve from the upper thigh to above the medial malleolus also were removed and fixed in 0.05 *M* phosphate buffer (pH 7.4) containing 1.5% glutaraldehyde and 3% formalin. After fixation, samples were taken every 4 cm along the nerves, embedded in paraffin or epoxy resin, cut, and stained as described for sural nerve specimens. Portions of the ventral and dorsal spinal roots were also fixed and processed in the same manner. Some of the quantitative aspects of the peripheral nervous system findings in Cases 2 and 3 were previously published.[18] Some descriptive pathologic findings in the peripheral nervous system in Cases 12 to 14 also were roughly described previously.[9]

Numbers and diameters of sympathetic ganglion neurons and

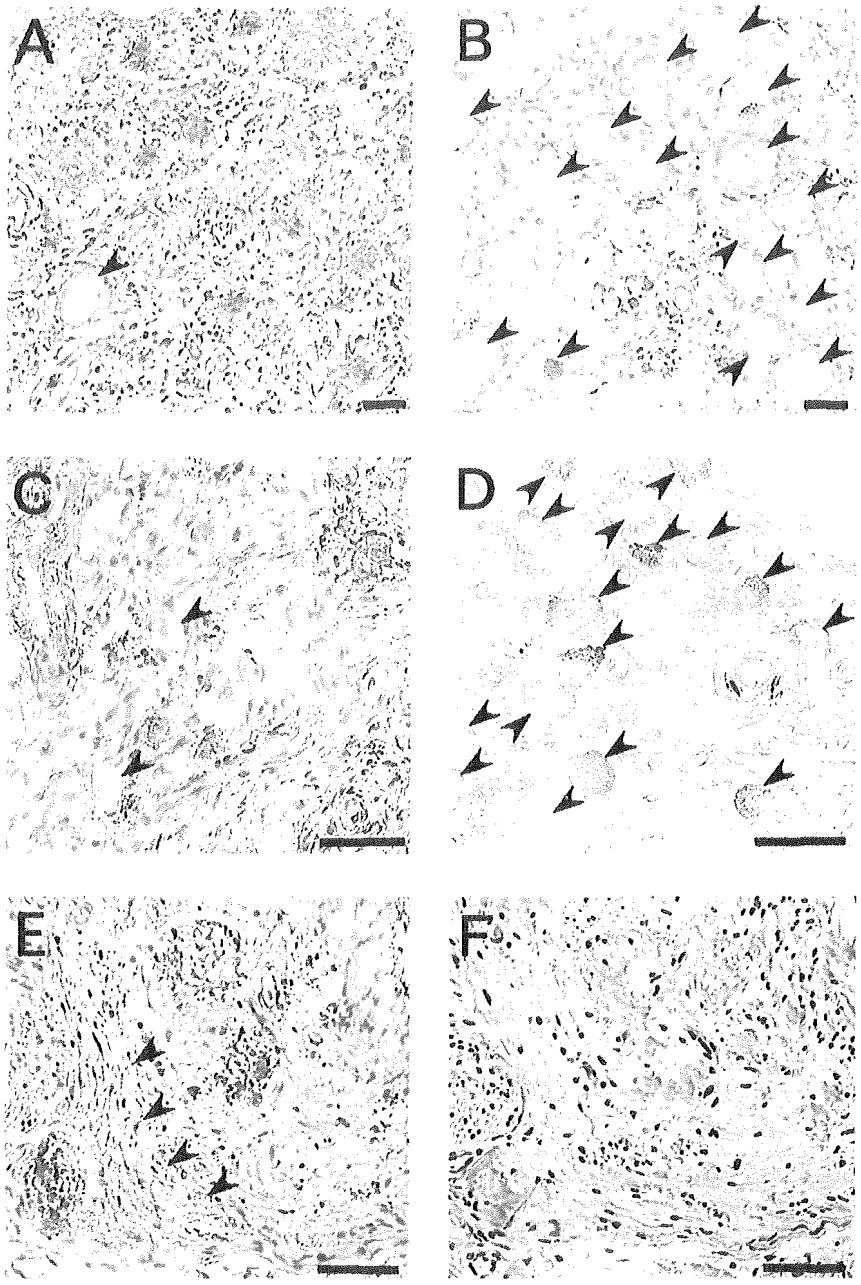

Figure 1. Representative postmortem findings in the peripheral nervous system. Amyloid deposits are identified by anti-human transthyretin antibody (A to E) or Congo red (F). (A, B) Dorsal root ganglia from early- and late-onset cases, respectively. (C, D) Sympathetic ganglia from early- and late-onset cases, respectively. In the dorsal root ganglia and sympathetic ganglia, amyloid deposition and neuronal cell loss are conspicuous in early-onset cases (A and C), whereas these are less severe in late-onset cases (B and D). Arrowheads indicate remaining neurons. (E, F) Consecutive specimens of the proximal part of sciatic nerve from a late-onset case. Amorphous material showing staining for transthyretin (E) but not with Congo red (F) is present in the subperineurial space (arrowheads). Bar = 40 μm.

dorsal root ganglion neurons were assessed using the image analyzer (Luzex FS). One hundred serial 10-μm-thick transverse sections at the middle portion of ganglia were prepared. Every tenth section was stained with the Klüver–Barrera method. Neurons showing obvious nucleoli in the sections were counted and measured to avoid split cell error. Number of neurons and area of ganglia on each section were assessed to calculate the density (neurons/mm^2). Values of neuronal cell density were expressed as means ± SD for these sections. For neuronal cell diameters, all neurons counted on 10 sections were measured. Values of neuronal cell diameter were expressed as means ± SD for these neurons. Control values for numbers and diameters of sympathetic and dorsal root ganglion neurons were obtained from four autopsy cases involving death from nonneurologic diseases.

Amounts of interstitial amyloid deposited in the parenchyma of various organs also were assessed using the Luzex FS analyzer. The proportion of area occupied by amyloid in each organ was determined as the extent of areas showing Congo red staining with emerald-green birefringence in polarized light and expressed as a percentage of the total transverse area. The proportion was assessed as the mean value for randomly selected areas covering at least 1 cm^2 of >10 sections. For nerve specimens, the proportion of area showing amyloid deposition to total endoneurial area was calculated. For the gastrointestinal tract, the proportion of area with amyloid deposition was assessed in the lamina muscularis mucosa.

Immunohistochemical assessment was performed with a peroxidase–antiperoxidase method using anti-human transthyretin antibody (Santa Cruz, CA) in consecutive deparaffinized sections.

Quantitative data, presented as means ± SD, were compared with control values. Statistical analyses were performed using the χ^2 test or the Mann–Whitney U test as appropriate. Values of p of <0.05 were considered to indicate significance.

Results. *Pathologic findings in sural nerve specimens.* In the early-onset cases, the density of large myelinated fibers was 914 ± 1,018 fibers/mm^2 (26% of age-matched normal control values) and that of small myelinated fibers was 451 ± 608 fibers/mm^2 (9% of age-matched normal control values), shown in table 2. Small myelinated fibers showed greater depletion than large myelinated fibers when myelinated fibers were not severely depleted overall (Cases 7 to 11). In late-onset cases, fiber size distribution

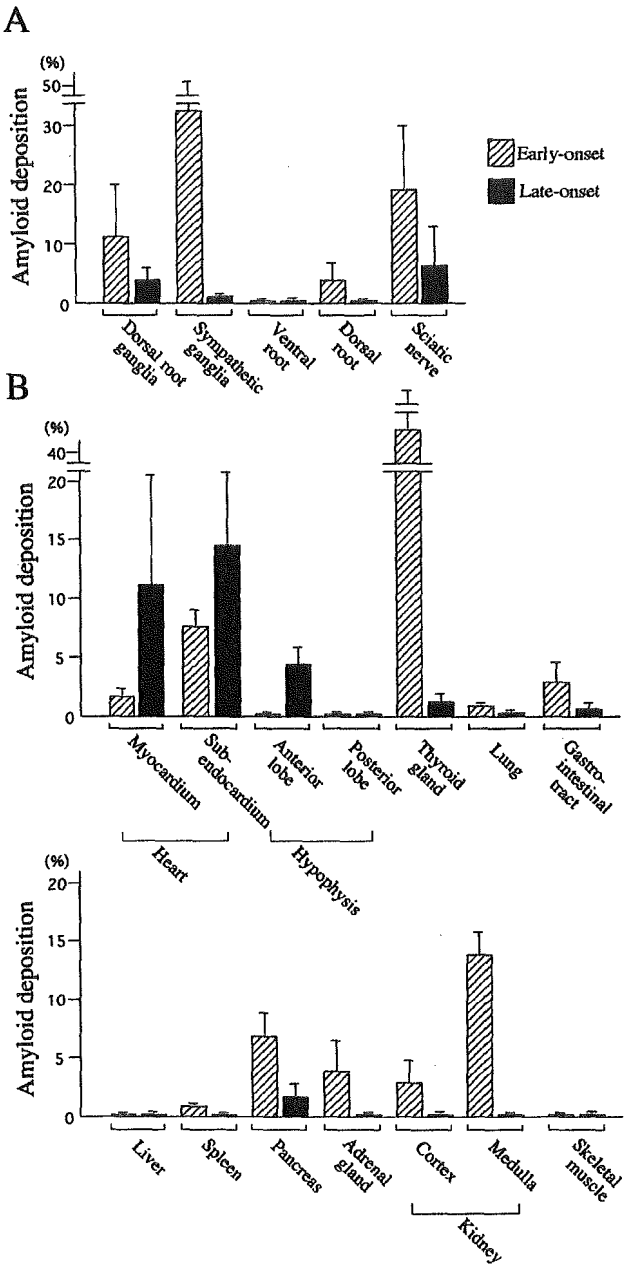

Figure 2. Amounts of interstitial amyloid deposited in the parenchyma of nervous system (A) and visceral organs (B). Hatched columns indicate mean values of early-onset cases (Cases 1 to 3), whereas filled columns indicate those of late-onset cases (Cases 12 to 14). Whiskers represent SDs. (A) Amyloid deposits in the nervous system are conspicuous in early-onset cases; these are less severe in late-onset cases. Amyloid deposition is more severe in sympathetic than dorsal root ganglia in early-onset cases, whereas the reverse pattern is seen in late-onset cases. (B) In early-onset cases, amyloid deposition is more prominent in the thyroid gland, gastrointestinal tract, pancreas, adrenal gland, and kidney than in late-onset cases. Amyloid deposition in early-onset cases is especially prominent in the thyroid gland and kidney, where deposition is scarce in late-onset cases. On the other hand, in late-onset cases, deposition is greater in the heart and anterior lobe of the hypophysis than in early-onset cases. Amyloid is scarce or absent in both groups in the posterior lobe of the pituitary gland, liver, and skeletal muscle.

of myelinated fibers, as indicated by the ratio of small to large myelinated fibers, was variable. Six cases (12, 14, 16 to 18, and 22) showed relative preservation of small myelinated fibers, whereas five cases (13, 15, 19 to 21) showed predominantly small-fiber loss as in early-onset cases. On average, density of large myelinated fibers was 333 ± 386 fibers/mm^2 (12% of age-matched normal control values) and that of small myelinated fibers was 789 ± 776 fibers/mm^2 (16% of age-matched normal control values). Axonal sprouting was scarce or absent in the early-onset group (5 ± 7/mm^2) but was relatively conspicuous in the late-onset group (92 ± 88/mm^2). Unmyelinated fibers were depleted more severely in the early- than the late-onset group (993 ± 1,305 vs 7,308 ± 5,417 fibers/mm^2; $p = 0.008$).

Amyloid deposition was scarce or absent in most cases in both groups, but relatively conspicuous deposition was observed in two of the early-onset cases (4 and 10). In both groups, amyloid was found in the endoneurium, both with and without relationship to small vessels.

Postmortem findings in the nervous system. Central nervous parenchyma was essentially intact in both groups, except that a small-cell carcinoma of the lung had metastasized to the cerebellum in Case 12, as previously described.[9,18] In the spinal cord, motor neurons as well as neurons in the Clarke columns were well preserved, and minimal to moderate myelinated fiber loss was observed in the posterior columns in both groups. Central chromatolysis was observed in spinal motor neurons in both groups. Amyloid deposits were not found in spinal cord parenchyma in any case.

In the dorsal root ganglia, amyloid deposits and neuronal cell loss were conspicuous in early-onset cases; these were less severe in late-onset cases (figures 1, A and B, and 2A). The mean diameter of remaining dorsal root ganglion neurons was larger in early-onset cases as compared with normal controls, suggesting predominant loss of small neurons (table 3). Mean neuronal cell diameters in late-onset cases were not notably different from those in normal controls, suggesting loss of neurons of all sizes. In the sympathetic ganglia, amyloid deposition and neuronal cell loss were very prominent in early-onset cases but less so in late-onset cases (see figures 1, C and D, and 2A). Size-selective neuronal cell loss was likely to be observed as in dorsal root ganglia (see table 3). Amyloid deposition and neuronal cell loss were more severe in sympathetic than dorsal root ganglia in early-onset cases, whereas the reverse pattern was seen in late-onset cases (see figure 2A and table 3). In the ventral spinal root, amyloid deposition was not apparent or only minimally present in both groups; likewise, myelinated fiber loss also was mild or not apparent in both groups. In the dorsal spinal root, amyloid deposition and myelinated fiber loss were moderately conspicuous in all early-onset cases but absent or minimal in late-onset cases. In sciatic and tibial nerves, amyloid deposition was more prominent in early-onset cases than the late-onset case (figure 3A). However, the late-onset case showed considerable myelinated fiber loss despite relative paucity of amyloid deposition (see figure 3B). In the median nerve, amyloid deposition also was more severe in early-onset cases than in the late-onset case, whereas myelinated fiber loss was more severe in the late-onset case than in early-onset cases. Amorphous material showing staining for transthyretin but not with Congo red was

Table 3 Neuronal cell loss and diameter in sympathetic and sensory ganglia

Case no.	Dorsal root ganglia		Sympathetic ganglia	
	Neuronal cell density, no./mm^2	Diameter of neurons in dorsal root ganglia, μm	Neuronal cell density, no./mm^2	Diameter of neurons in sympathetic ganglia, μm
Early-onset group				
1	4.0 ± 0.9	54.3 ± 8.6	4.2 ± 2.2	24.3 ± 3.8
2	1.9 ± 1.2	53.7 ± 8.8	4.0 ± 1.6	23.7 ± 4.2
3	2.6 ± 1.0	56.0 ± 9.0	1.6 ± 1.4	24.5 ± 3.3
Late-onset group				
12	7.5 ± 1.6	46.2 ± 11.4	46.2 ± 7.4	22.9 ± 4.6
13	4.8 ± 1.2	45.4 ± 9.1	44.8 ± 6.2	19.8 ± 4.6
14	5.8 ± 1.3	49.9 ± 11.4	ND	ND
Controls, n = 4	10.2 ± 3.2	48.3 ± 16.3	60.4 ± 6.6	20.0 ± 4.2

Values of neuronal cell density were expressed as means ± SD for densities on 10 sections as described in Patients and Methods. Values of neuronal cell diameter were expressed as means ± SD for all neurons counted on 10 sections. Control values were obtained from four autopsied cases.

ND = not determined.

abundant in the subperineurial space of the nerve trunk in the late-onset case (see figure 1, E and F), being less plentiful in early-onset cases.

Pathologic findings in visceral organs. In early-onset cases, amyloid deposition was more prominent in the thyroid gland, gastrointestinal tract, pancreas, adrenal gland, and kidney than in late-onset cases (figures 2B and 4). Amyloid deposition in early-onset cases was especially prominent in the thyroid gland and kidney, where deposition was scarce in late-onset cases. On the other hand, in late-onset cases, deposition was greater in the heart and the anterior pituitary lobe than in early-onset cases. Amyloid was scarce or absent in both groups in the posterior lobe of the pituitary gland, liver, and skeletal muscle. The heart weighed 420, 440, and 450 g in early-onset cases, whereas in late-onset patients dying of heart failure, it was 690 and 700 g. In a late-onset patient who died of lung cancer and had relatively short clinical duration of amyloid neuropathy, the heart weight was 380 g. In early-onset cases, cardiac amyloid deposition was prominent in the atrium and the subendocardial region. In the myocardium, amyloid was observed mainly in relation to walls of vessels, particularly arterioles. In the subendocardial layer, myocardial cells showed atrophy, degeneration, and eventual cell loss, producing a histologic picture of amyloid rings (see figure 4A). Among late-onset cases, amyloid was prominent throughout myocardium in two cases (13 and 14), whereas amyloid rings or atrophy of the myocardium was not apparent in any case (see figure 4B). The anterior lobe of the hypophysis showed scarce or no amyloid deposition in early-onset cases, but marked parenchymal deposition was observed in late-onset cases (see figure 4, C and D).

Discussion. In this study, we compared pathologic features of early-onset FAP TTR Met30 cases from endemic foci with those of late-onset cases from non-endemic areas. In anecdotal report of pathologic findings in FAP TTR Met30 patients presenting beyond age 50,[25] the distribution of amyloid deposition differed slightly from findings in the current study. Differences may be attributable to inclusion of late-onset cases from endemic foci in that report; these patients show clinical features similar to early-onset cases in endemic foci.[11] The current study demonstrated that pathologic features of the two groups differed, as has been shown for clinical features.[9-11]

The characteristic finding in early-onset cases was predominant loss of small fibers, including unmyelinated fibers; this agrees with previous reports.[26,27] On the other hand, fiber loss patterns in our late-onset cases were variable; half of the cases showed predominantly small-fiber loss as in early-onset cases, whereas others showed relative preservation of small myelinated fibers. As a whole, the total number of myelinated fibers was more severely reduced in late- than early-onset cases. This difference correlated well with the prominent sensory dissociation noted in early-onset cases in contrast to impairment of all modalities in late-onset cases.[3,9,11] The finding that amyloid deposition and neuronal cell loss were more severe in sympathetic than sensory ganglia in early-onset cases—with the reverse pattern seen in late-onset cases—also correlated with the severity of autonomic symptoms.[3,7-9,11] Furthermore, preferential loss of small neurons in the sensory ganglia in early-onset cases and loss of neurons of all sizes in late-onset cases, as suggested by the mean diameter of remaining neurons, corresponded to clinical differences in sensory involvement. Amyloid deposition and atrophy of myocardial cells in the atrium and subendocardial layer of the myocardium, where the cardiac conduction system is located, explains a more frequent occurrence of cardiac conduction abnormalities and need for pacemaker implantation in early- than late-onset cases.[3,11] On the other hand, diffuse deposition of amyloid with ventricular wall thickening agrees well with frequent observations of cardiac hypertrophy and occur-

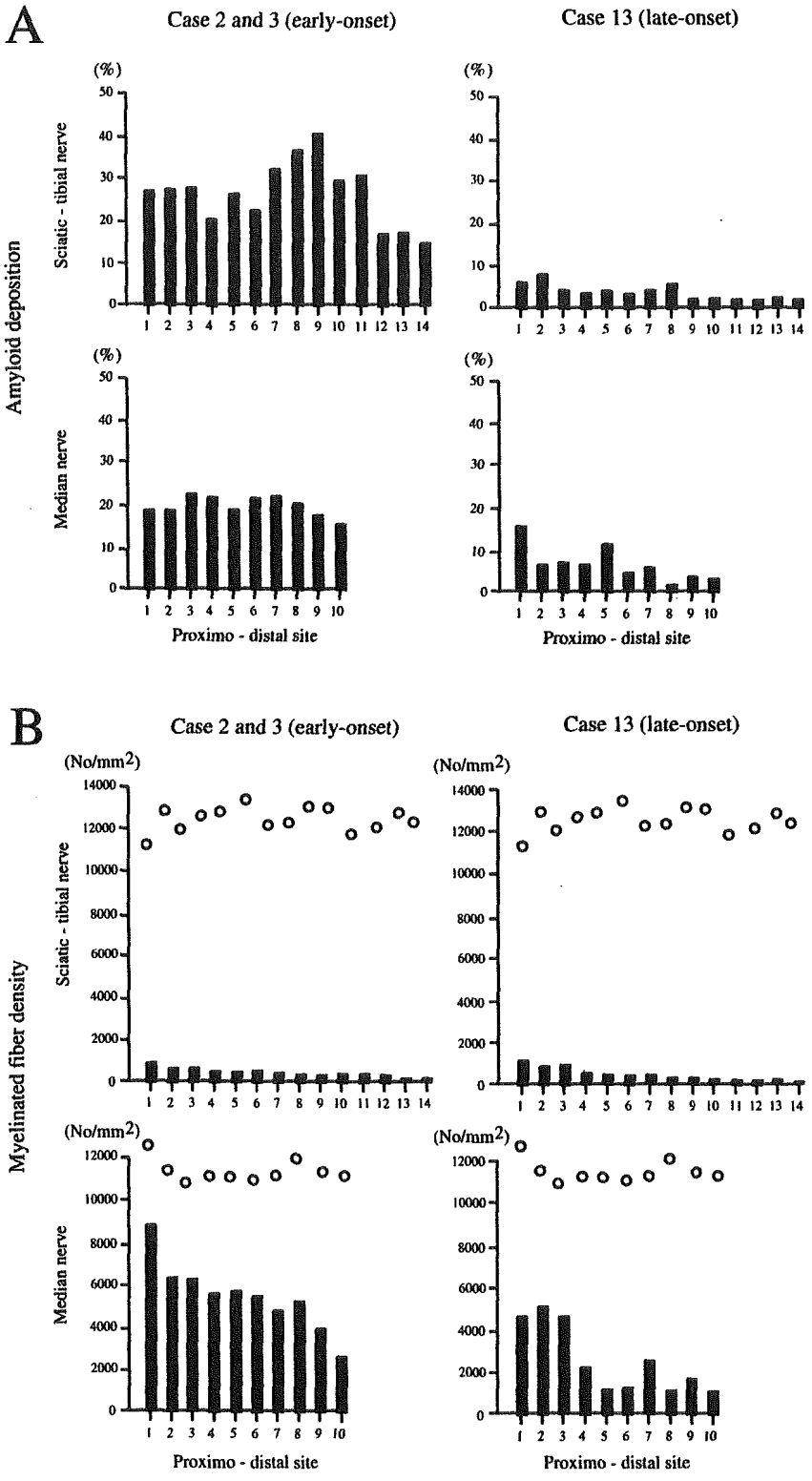

Figure 3. Proportion of amyloid deposition in the endoneurium (A) and density of myelinated fibers (B) in consecutive portions of the sciatic/tibial and median nerves from early-onset cases (Cases 2 and 3) and late-onset case (Case 13). Values for early-onset cases are represented as the means of Cases 2 and 3. Open circles represent normal control values obtained from a subject with nonneurologic disease. In sciatic and tibial nerves, amyloid deposition is more prominent in early-onset cases than in the late-onset case. However, the late-onset case showed considerable myelinated fiber loss despite relative paucity of amyloid deposition. In the median nerve, amyloid deposition also is more severe in early-onset cases than in the late-onset case, whereas myelinated fiber loss is more severe in the late-onset case than in early-onset cases.

rence of heart failure in late-onset cases.[9] Thus, differences in clinical features reported between early- and late-onset FAP TTR Met30 corresponded well to pathologic differences.

A question remains as to why the severity and distribution pattern of amyloid deposition differ between early- and late-onset cases. A longer interval from onset of neuropathic symptoms to autopsy in the early-onset group may explain some of the pathologic differences. The peripheral nervous system, thyroid gland, gastrointestinal tract, pancreas, adrenal gland, and kidney showed more severe amyloid deposition in the early-onset group, consistent with a longer duration of illness. However, the heart and hypophysis showed more prominent deposition in the late-onset group, which had a shorter clinical disease duration. The diffuse amyloid deposition observed in the ventricular myocardium in late-onset cases is

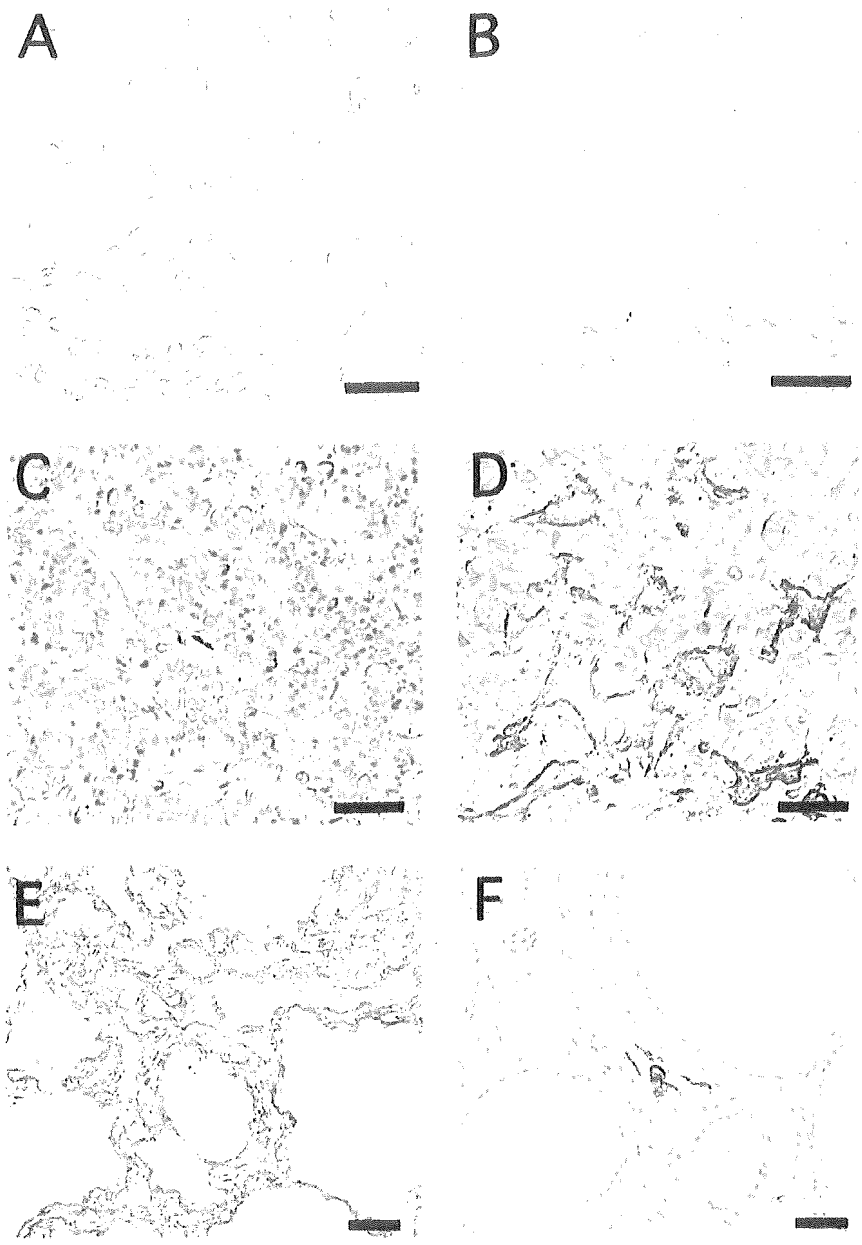

Figure 4. Representative pathologic findings in the visceral organs from early-onset cases (left) and late-onset cases (right). Amyloid deposits are identified by anti-human transthyretin antibody. (A, B) The heart. In the subendocardial layer of an early-onset case (A), myocardial cells show atrophy and amyloid rings are present. In late-onset cases, amyloid is prominent throughout myocardium (B). Amyloid rings or atrophy of the myocardium is not apparent as in (A). (C, D) Anterior lobe of the pituitary gland. Amyloid deposition is scarce in early-onset cases (C), whereas it is conspicuous in late-onset cases (D). (E, F) The thyroid gland. Amyloid deposition was especially prominent in early-onset cases (E), but it was scarce in late-onset cases (F). Bar = 40 μm.

similar to that of senile cardiac amyloidosis with deposition of normal transthyretin protein.[28] Age-related accumulation of amyloid in the interstitium of the anterior lobe of the pituitary gland also has been reported.[29-31] These observations suggest that age-dependent changes in the microenvironment of interstitial tissues in various organs determine the severity and distribution pattern of amyloid deposition in each group. For example, properties of extracellular matrix components including proteoglycans and glycosaminoglycans, which may become components of amyloid,[32] show organ-specific changes with age.[33,34] Interestingly, the posterior lobe of the hypophysis, the liver, and skeletal muscle did not show detectable amyloid deposition in cases with either age at onset. Mechanisms of underlying organ-specific, age-related amyloid deposition still need to be elucidated, but age at onset itself may influence some of the organ-specific amyloid deposition patterns.

Another question remaining is why size dependence of axonal and neuronal cell loss differed between early- and late-onset cases. Even after taking axonal sprouting into account, small myelinated and unmyelinated fibers seemed relatively well preserved in many late-onset cases. Although the pathogenesis of peripheral neuropathy in amyloidosis has not yet been clarified, possibilities might include ischemia from obliteration or dysfunction of small vessels supplying nerves,[35,36] nerve fiber compression or infiltration by amyloid deposits,[26,37] or toxic effects of amyloid precursors.[38-40] Experiments in animals as well as human studies suggest that the nonfibrillar form of transthyretin is present in tissues and exerts cytotoxicity, including oxidative stress,[40] before the congophilic fibrillar form of amyloid can be seen.[38,41]

The concept that a nonfibrillar precursor of amyloid can exert toxic effects can be extended to other pathologic conditions where amyloid is considered pathogenetically important, including Alzheimer disease.[42-45] In our study, amyloid was not deposited in late-onset cases until patients had become elderly, considering that amyloid deposition was scarce or absent in sural nerve biopsy specimens. Accumulation of amyloid may progress rapidly once initiated. Abundant nerve fiber regeneration despite scarce amyloid deposition was observed in most sural nerve biopsy specimens from our late-onset cases, indicating that axons had been degenerating long before amyloid deposition occurred in these cases. At autopsy, less amyloid deposition but severe myelinated fiber loss in nerve trunks from a late-onset case in comparison with early-onset cases support this view. Furthermore, amorphous material staining with anti-transthyretin antibody but not with Congo red, indicating presence of the nonfibrillar amyloid precursor, was more abundant in the late-onset case. Taken together, these observations support cytotoxicity from nonfibrillar transthyretin affecting all sizes of axons and neurons prior to deposition of congophilic amyloid in late-onset cases. In early-onset cases, amyloid deposition was likely to have been severe even in early stages, judging from amounts of amyloid observed. Nerve fiber compression by amyloid deposits could cause predominantly small-fiber loss, as previously suggested.[26] Differential duration of exposure to a toxic amyloid precursor may result in pathologically different modes of axonal and neuronal cell loss.

References

1. Andrade C. A peculiar form of peripheral neuropathy. Familial atypical generalized amyloidosis with special involvement of the peripheral nerves. Brain 1952;75:408–427.
2. Benson MD, Cohen AS. Generalized amyloid in a family of Swedish origin. A study of 426 family members in seven generations of a new kinship with neuropathy, nephropathy, and central nervous system involvement. Ann Intern Med 1977;86:419–424.
3. Ikeda S, Hanyu N, Hongo M, et al. Hereditary generalized amyloidosis with polyneuropathy: clinicopathological study of 65 Japanese patients. Brain 1987;110:315–337.
4. Nakazato M, Shiomi K, Miyazato M, Matsukura S. Type 1 familial amyloidotic polyneuropathy in Japan. Intern Med 1992;31:1335–1338.
5. Sousa A, Coelho T, Barros J, Sequeiros J. Genetic epidemiology of familial amyloidotic polyneuropathy (FAP)-type I in Povoa do Varzim and Vila do Conde (north of Portugal). Am J Med Genet 1995;60:515–521.
6. Reilly MM, Adams D, Booth DR, et al. Transthyretin gene analysis in European patients with suspected familial amyloid polyneuropathy. Brain 1995;118:849–856.
7. Ando Y, Araki S, Shimoda O, Kano T. Role of autonomic nerve functions in patients with familial amyloidotic polyneuropathy as analyzed by laser Doppler flowmetry, capsule hydrograph, and cardiographic R-R interval. Muscle Nerve 1992;15:507–512.
8. Ando Y, Suhr OB. Autonomic dysfunction in familial amyloid polyneuropathy (FAP). Amyloid Int J Exp Clin Invest 1998;5:288–300.
9. Misu K, Hattori N, Nagamatsu M, et al. Late-onset familial amyloid polyneuropathy type I (transthyretin Met 30-associated familial amyloid polyneuropathy) unrelated to endemic focus in Japan; clinicopathological and genetic features. Brain 1999;122:1951–1962.
10. Misu K, Hattori N, Ando Y, Ikeda S, Sobue G. Anticipation in early- but not late-onset familial amyloid polyneuropathy (TTR met 30) in Japan. Neurology 2000;55:451–452.
11. Koike H, Misu K, Ikeda S, et al. Type I (transthyretin Met30) familial amyloid polyneuropathy in Japan: early- versus late-onset form. Arch Neurol 2002;59:1771–1776.
12. Sobue G, Koike H, Misu K, et al. Clinicopathologic features of early- and late-onset FAP type I (FAP ATTR Val30Met) in Japan. Amyloid J Protein Folding Disord 2003;1(suppl):32–38.
13. Coelho T, Sousa A, Lourenco E, Ramalheira J. A study of 159 Portuguese patients with familial amyloidotic polyneuropathy (FAP) whose parents were both unaffected. J Med Genet 1994;31:293–299.
14. Saravia MJ, Costa PP, Goodman DS. Genetic expression of a transthyretin mutation in typical and late-onset Portuguese families with familial amyloidotic polyneuropathy. Neurology 1986;36:1413–1417.
15. Sasaki Y, Yoshioka K, Tanahashi H, Furuya H, Sasaki H. Human transthyretin (prealbumin) gene and molecular genetics of familial amyloidotic polyneuropathy. Mol Biol Med 1989;6:161–168.
16. Sobue G, Yasuda T, Mitsuma T, Loss AH, Pleasure D. Expression of nerve growth factor receptor in human peripheral neuropathies. Ann Neurol 1988;24:64–72.
17. Sobue G, Hashizume Y, Mukai E, et al. X-linked recessive bulbospinal neuronopathy, a clinicopathological study. Brain 1989;112:209–232.
18. Sobue G, Nakao N, Murakami K, et al. Type I familial amyloid polyneuropathy. A pathological study of the peripheral nervous system. Brain 1990;113:903–919.
19. Hattori N, Ichimura M, Nagamatsu M, et al. Clinicopathological features of Churg–Strauss syndrome-associated neuropathy. Brain 1999; 122:427–439.
20. Koike H, Mori K, Misu K, et al. Painful alcoholic polyneuropathy with predominant small-fiber loss and normal thiamine status. Neurology 2001;56:1727–1732.
21. Koike H, Iijima M, Sugiura M, et al. Alcoholic neuropathy is clinicopathologically distinct from thiamine-deficiency neuropathy. Ann Neurol 2003;54:19–29.
22. Hattori N, Yamamoto M, Yoshihara T, et al. Demyelinating and axonal features of Charcot–Marie–Tooth disease with mutations of myelin-related proteins (PMP22, MPZ and Cx32): a clinicopathological study of 205 Japanese patients. Brain 2003;126:134–151.
23. Dyck PJ, Giannini C, Lais A. Pathologic alterations of nerves. In: Dyck PJ, Thomas PK, Griffin JW, Low PA, Poduslo JF, eds. Peripheral neuropathy. 3rd ed. Philadelphia: Saunders, 1993:514–595.
24. Nagamatsu M, Terao S, Misu K, et al. Axonal and perikaryal involvement in chronic inflammatory demyelinating polyneuropathy. J Neurol Neurosurg Psychiatry 1999;66:727–733.
25. Takahashi K, Sakashita N, Ando Y, Suga M, Ando M. Late onset type I familial amyloidotic polyneuropathy: presentation of three autopsy cases in comparison with 19 autopsy cases of the ordinary type. Pathol Int 1997;47:353–359.
26. Said G, Ropert A, Faux N. Length-dependent degeneration of fibers in Portuguese amyloid polyneuropathy: a clinicopathologic study. Neurology 1984;34:1025–1032.
27. Takahashi K, Yi S, Kimura Y, Araki S. Familial amyloidotic polyneuropathy type 1 in Kumamoto, Japan: a clinicopathologic, histochemical, immunohistochemical, and ultrastructural study. Hum Pathol 1991;22: 519–527.
28. Olson LJ, Gertz MA, Edwards WD, et al. Senile cardiac amyloidosis with myocardial dysfunction. Diagnosis by endomyocardial biopsy and immunohistochemistry. N Engl J Med 1987;317:738–742.
29. Tashima T, Kitamoto T, Tateishi J, Ogomori K, Nakagaki H. Incidence and characterization of age related amyloid deposits in the human anterior pituitary gland. Virchows Arch A Pathol Anat Histopathol 1988;412:323–327.
30. Röcken C, Eick B, Saeger W. Senile amyloidosis of the pituitary and adrenal glands. morphological and statistical investigations. Virchows Arch 1996;429:293–299.
31. Westermark P, Eriksson L, Engstrom U, Enestrom S, Sletten K. Prolactin-derived amyloid in the aging pituitary gland. Am J Pathol 1997;150:67–73.
32. Magnus JH, Stenstad T. Proteoglycans and the extracellular matrix in amyloidosis. Amyloid J Exp Clin Invest 1997;4:121–134.
33. Nakayama Y, Narita T, Mori A, Uesaka S, Miyazaki K, Ito H. The effects of age and sex on chondroitin sulfates in normal synovial fluid. Arthritis Rheum 2002;46:2105–2108.
34. Carrino DA, Onnerfjord P, Sandy JD, et al. Age-related changes in the proteoglycans of human skin. Specific cleavage of decorin to yield a major catabolic fragment in adult skin. J Biol Chem 2003;278:17566–17572.
35. Hanyu N, Ikeda S, Nakadai A, Yanagisawa N, Powell HC. Peripheral nerve pathological findings in familial amyloid polyneuropathy: a correlative study of proximal sciatic nerve and sural nerve lesions. Ann Neurol 1989;25:340–350.
36. Berghoff M, Kathpal M, Khan F, Skinner M, Falk R, Freeman R. Endothelial dysfunction precedes C-fiber abnormalities in primary (AL) amyloidosis. Ann Neurol 2000;53:725–730.
37. Dyck PJ, Lambert EH. Dissociated sensation in amyloidosis. Compound action potential, quantitative histologic and teased-fiber, and electron microscopic studies of sural nerve biopsies. Arch Neurol 1969;20:490–507.
38. Sousa MM, Cardoso I, Fernandes R, Guimaraes A, Saraiva MJ. Deposition of transthyretin in early stages of familial amyloidotic polyneuropathy: evidence for toxicity of nonfibrillar aggregates. Am J Pathol 2001; 159:1993–2000.
39. Andersson K, Olofsson A, Nielsen EH, Svehag SE, Lundgren E. Only amyloidogenic intermediates of transthyretin induce apoptosis. Biochem Biophys Res Commun 2002;294:309–314.

40. Fiszman ML, Di Egidio M, Ricart KC, et al. Evidence of oxidative stress in familial amyloidotic polyneuropathy type 1. Arch Neurol 2003;60: 593–597.
41. Sousa MM, Fernandes R, Palha JA, Taboada A, Vieira P, Saraiva MJ. Evidence for cytotoxic aggregates in transgenic mice for human transthyretin Leu55Pro. Am J Pathol 2002;161:1935–1948.
42. LaFerla FM, Tinkle BT, Bieberich CJ, Haudenschild CC, Jay G. The Alzheimer's Abeta peptide induces neurodegeneration and apoptotic cell death in transgenic mice. Nat Genet 1995;9:21–30.
43. Hartley DM, Walsh DM, Ye CP, et al. Protofibrillar intermediates of amyloid beta-protein induce acute electrophysiological changes and progressive neurotoxicity in cortical neurons. J Neurosci 1999;19:8876–8884.
44. McLean CA, Cherny RA, Fraser FW, et al. Soluble pool of Abeta amyloid as a determinant of severity of neurodegeneration in Alzheimer's disease. Ann Neurol 1999;46:860–866.
45. Kayed R, Head E, Thompson JL, et al. Common structure of soluble amyloid oligomers implies common mechanism of pathogenesis. Science 2003;300:486–489.

Journal of Neurochemistry, 2004, **89**, 64–72 doi:10.1046/j.1471-4159.2003.02289.x

Dorfin prevents cell death by reducing mitochondrial localizing mutant superoxide dismutase 1 in a neuronal cell model of familial amyotrophic lateral sclerosis

Hideyuki Takeuchi, Jun-ichi Niwa, Nozomi Hishikawa, Shinsuke Ishigaki, Fumiaki Tanaka, Manabu Doyu and Gen Sobue

Department of Neurology, Nagoya University Graduate School of Medicine, 65 Tsurumai-cho, Showa-ku, Nagoya 466-8550, Japan

Abstract

Dorfin is a RING-finger type ubiquitin ligase for mutant superoxide dismutase 1 (SOD1) that enhances its degradation. Mutant SOD1s cause familial amyotrophic lateral sclerosis (FALS) through the gain of unelucidated toxic properties. We previously showed that the accumulation of mutant SOD1 in the mitochondria triggered the release of cytochrome *c*, followed by the activation of the caspase cascade and induction of neuronal cell death. In the present study, therefore, we investigated whether Dorfin can modulate the level of mutant SOD1 in the mitochondria and subsequent caspase activation. We showed that Dorfin significantly reduced the amount of mutant SOD1 in the mitochondria, the release of cytochrome *c* and the activation of the following caspase cascade, thereby preventing eventual neuronal cell death in a neuronal cell model of FALS. These results suggest that reducing the accumulation of mutant SOD1 in the mitochondria may be a new therapeutic strategy for mutant SOD1-associated FALS, and that Dorfin may play a significant role in this.

Keywords: amyotrophic lateral sclerosis, Dorfin, mitochondria, neuronal cell death, superoxide dismutase 1, ubiquitin ligase.

J. Neurochem. (2004) **89**, 64–72.

Amyotrophic lateral sclerosis (ALS) is a fatal neurodegenerative disease caused by selective death of motor neurons. Approximately 10% of ALS cases are familial (FALS). Missense mutations in the gene coding superoxide dismutase 1 (SOD1) are responsible for approximately 20% of FALS cases (Rosen *et al.* 1993; Hirano 1996) through the gain of unelucidated toxic properties (Yim *et al.* 1996).

Many reports have documented that the mitochondria are involved in the pathogenic process in mutant SOD1-associated FALS. Mitochondrial degeneration, including swelling, dilatation and vacuolization, is an early characteristic pathological feature of FALS and FALS transgenic (Tg) mice models with SOD1 mutations (Dal Canto and Gurney 1994; Wong *et al.* 1995; Hirano 1996; Kong and Xu 1998; Jaarsma *et al.* 2000; Higgins *et al.* 2003). Recently, it was demonstrated that SOD1, considered to be a cytosolic enzyme, exists in the mitochondria (Sturtz *et al.* 2001; Okado-Matsumoto and Fridovich 2001; Higgins *et al.* 2002), and that the mitochondrial vacuoles in mutant SOD1 Tg mice were lined with mutant SOD1 (Jaarsma *et al.* 2001; Higgins *et al.* 2003). Many studies have suggested that the programmed cell death (PCD) pathway contributes to motor neuron death in FALS (Durham *et al.* 1997; Martin 1999; Li *et al.* 2000; Pasinelli *et al.* 2000; Guégan *et al.* 2001; Kriz *et al.* 2002; Raoul *et al.* 2002; Zhu *et al.* 2002). Moreover, we previously reported that accumulation of mutant SOD1 in the mitochondria triggered the release of mitochondrial cytochrome *c*, which subsequently activated the caspase cascade and induced neuronal cell death (Takeuchi *et al.* 2002a). Taken together, these results suggest that the accumulation of mutant SOD1 in the mitochondria is critical in the pathogenesis of mutant SOD1-associated FALS.

Received September 23, 2003; revised manuscript received November 17, 2003; accepted November 24, 2003.

Address correspondence and reprint requests to Gen Sobue, Department of Neurology, Nagoya University Graduate School of Medicine, 65 Tsurumai-cho, Showa-ku, Nagoya 466–8550, Japan.
E-mail: sobueg@med.nagoya-u.ac.jp

Abbreviations used: ALS, amyotrophic lateral sclerosis; COX, cytochrome *c* oxidase; DMEM, Dulbecco's modified Eagle's medium; E3, ubiquitin ligase; EGFP, enhanced green fluorescent protein; FALS, familial amyotrophic lateral sclerosis; MTS, 3-(4,5-dimethyl-thiazol-2yl)-5-(3-carboxymethoxyphenyl)-2-(4-sulfophenyl)-2H-tetrazolium; PCD, programmed cell death; PI, propidium iodide; SOD1, superoxide dismutase 1; Tg, transgenic.

Dorfin is the product of a gene that we cloned from the anterior horn tissue of the human spinal cord (Niwa *et al.* 2001); it contains a RING-finger/IBR motif (Niwa *et al.* 2001) at its N-terminus. It was reported that a distinct subclass of RING-finger/in-between RING-fingers (IBR) motif-containing proteins represents a new ubiquitin ligase (E3) family that interacts specifically with distinct ubiquitin-conjugating enzymes (Moynihan *et al.* 1999; Ardley *et al.* 2001). Dorfin is a juxtanuclearly located E3 that ubiquitylates various SOD1 mutants derived from patients with FALS, and enhances the degradation of mutant SOD1 (Niwa *et al.* 2002). Whether Dorfin can modulate the protein level of mutant SOD1 in the mitochondria, and the subsequent activation of the mitochondrial caspase cascade, is an important and interesting question.

Here we show that Dorfin significantly reduced the amount of mutant SOD1 in mitochondria, the release of cytochrome *c* from mitochondria into the cytosol and the subsequent activation of the caspase cascade, thereby preventing the eventual neuronal cell death in a neuronal cell model of FALS. These results suggest that reducing mutant SOD1 in the mitochondria may be a useful strategy for the treatment of mutant SOD1-associated FALS, and that Dorfin might play a significant role in this.

Materials and methods

Plasmids

Non-organelle-oriented plasmids expressing the enhanced green fluorescent protein (EGFP)-tagged human SOD1 (wild type, mutant G93A, and G85R) were described previously (Takeuchi *et al.* 2002a,b). These vectors express SOD1-EGFP fusion proteins ubiquitously in each organelle (Takeuchi *et al.* 2002a). They were designated Cyto-WT, Cyto-G93A and Cyto-G85R respectively. Mitochondria-oriented plasmids expressing EGFP-tagged human SOD1 (wil dtype, mutant G93A and G85R) with mitochondrial localizing signals were generated as described previously (Takeuchi *et al.* 2002a). These vectors express SOD1-EGFP fusion proteins mainly in the mitochondria (Takeuchi *et al.* 2002a). They were designated Mito-WT, Mito-G93A and Mito-G85R respectively. The plasmid pcDNA3.1/HisMax-Dorfin, which expresses Xpress-tagged Dorfin, was also described previously (Niwa *et al.* 2001). As a control, we used pCMV-β vector expressing LacZ (Clontech, Palo Alto, CA, USA). All constructs used here were confirmed by DNA sequence analysis.

Cell culture

Mouse neuroblastoma cell line Neuro2a cells were maintained in Dulbecco's modified Eagle's medium (DMEM) (Invitrogen Corp., Carlsbad, CA, USA) supplemented with 10% fetal calf serum (Invitrogen Corp.) as described previously (Takeuchi *et al.* 2002b). They were cultured on Laboratory-Tec II four-well chamber slides (Nalge Nunc International, Rochester, NY, USA) coated with poly-L-lysine (Sigma, St Louis, MO, USA). Transient expression of SOD1 plasmids (0.1 μg of DNA/well) and pcDNA3.1/His Max-Dorfin or pCMV-β (0.3 μg of DNA/well) in Neuro2a cells (2×10^4 cells/well) was accomplished with LipofectAMINE PLUS reagent (Invitrogen Corp.). After incubation for 3 h with transfection reagents, transfected cells were cultured in differentiation medium (DMEM supplemented with 1% fetal calf serum and 20 μM retinoic acid). To detect Xpress-Dorfin fusion protein, 0.5 μM proteasome inhibitor MG132 (Sigma) was added 16 h before collection, as described previously (Niwa *et al.* 2001).

Cell fractionation

At each time point (0, 24 and 48 h) after transfection, cells were collected and gently homogenized with a Dounce homogenizer in cold buffer [250 mM sucrose, 10 mM Tris-HCl pH 7.5, 5 mM $MgCl_2$, 2 mM EDTA and protease inhibitor cocktail (Complete Mini EDTA-free; Roche Diagnostics, Basel, Switzerland)]. Cell fractionation was performed as described previously (Takeuchi *et al.* 2002a). To verify the fractionation, each fraction was subjected to western blotting for cytochrome *c* oxidase (COX) as a mitochondrial marker using anti-COX subunit IV mouse monoclonal antibody (1 : 1000; Molecular Probes, Eugene, OR, USA), and β-actin as a cytosolic marker using anti-β-actin mouse monoclonal antibody (1 : 5000; Sigma).

Western blot analysis

The protein concentration was determined with a DC protein assay kit (Bio-Rad Laboratories, Hercules, CA, USA) and western blotting was done as described previously (Takeuchi *et al.* 2002b). To evaluate the level of mitochondrially localized SOD1-EGFP fusion proteins, 20 μg protein from the mitochondrial fraction was loaded. For analyzing the release of cytochrome *c* from the mitochondria into the cytosol, 20 μg protein from the mitochondrial fraction or the cytosolic fraction was loaded.

To assess the levels of SOD1-EGFP fusion proteins, Xpress-Dorfin fusion proteins and the activation of caspase-9 and caspase-3, cells were collected at each time point (0, 24 and 48 h) after transfection, and lysed in TNES buffer (50 mM Tris-HCl pH 7.5, 150 mM NaCl, 1% NP-40, 2 mM EDTA, 0.1% sodium dodecyl sulfate and protease inhibitor cocktail) as described previously (Takeuchi *et al.* 2002a). For the analysis, 20 μg protein from the total lysate was loaded.

The primary antibodies used were as follows: anti-SOD1 rabbit polyclonal antibody (1 : 10 000; StressGen Biotechnologies, Victoria, BC, Canada), anti-Xpress mouse monoclonal antibody (1 : 5000; Invitrogen Corp.), anti-caspase-3 rabbit polyclonal antibody and anti-caspase-9 rabbit polyclonal antibody (1 : 1000; Cell Signaling, Beverly, MA, USA) and anti-cytochrome *c* mouse monoclonal antibody (1 : 1000; Pharmingen, San Diego, CA, USA). After overnight incubation with primary antibodies at 4°C, each blot was probed with horseradish peroxidase-conjugated anti-rabbit IgG and anti-mouse IgG (1 : 5000; Amersham Biosciences, Piscataway, NJ, USA). Blots were then visualized with ECL Plus western blotting detection reagents (Amersham Biosciences). The signal intensity was quantified by densitometry using NIH Image 1.63 software.

Immunocytochemistry

At each time point (0, 24 and 48 h) after transfection, cells were fixed with 4% paraformaldehyde for 30 min on ice and then

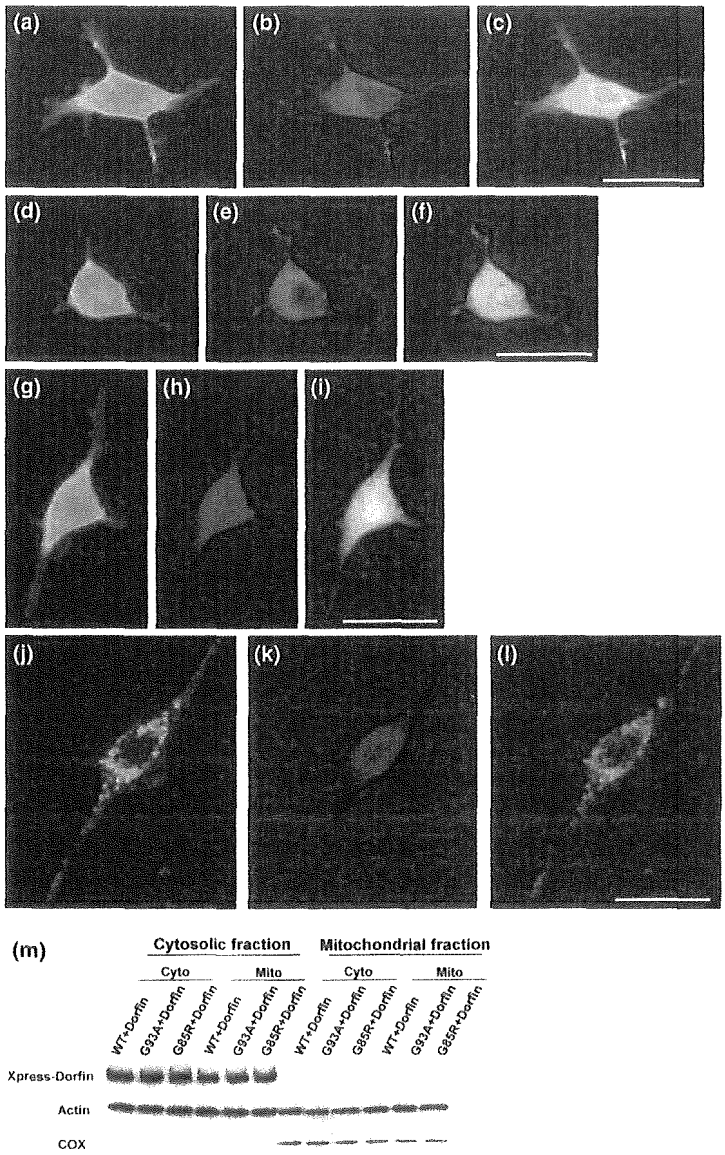

Fig. 1 Subcellular localization of SOD1-EGFP and Xpress-Dorfin in Neuro2a cells. (a–l) *Confocal laser scanning microscopic* images at 48 h after transfection. (m) Fractionation analysis of Xpress-Dorfin fusion protein. (a–c) Cyto-WT + Xpress-Dorfin, (d–f) Cyto-G93A + Xpress-Dorfin, (g–l) Cyto-G85R + Xpress-Dorfin; (j–l) Mito-G93A + Xpress-Dorfin. SOD1-EGFP fusion proteins (green; a, d and g) and Xpress-Dorfin fusion proteins (red; b, e and h) were observed ubiquitously in the cells with Cyto-SOD1 containing no organelle-oriented signals. SOD1-EGFP fusion proteins and Xpress-Dorfin fusion proteins were co-localized (yellow; c, f and i). In contrast, in the cells with Mito-SOD1, SOD1-EGFP fusion proteins were observed in the mitochondria (green; j) and Xpress-Dorfin fusion proteins (red; k) were observed mainly in the cytoplasm. They were not co-localized in the cells with Mito-SOD1 (l). Cells were counterstained with TO-PRO-3 (blue). Scale bars, 10 μm. Western blots also revealed that Xpress-Dorfin fusion proteins were absent in the mitochondrial fraction (m).

permeabilized with 0.05% Triton X-100 at room temperature for 10 min. They were stained with the anti-Xpress mouse monoclonal antibody (1 : 5000; Invitrogen Corp.) at 4°C overnight. They were subsequently stained with Alexa-568-conjugated secondary antibody (1 : 5000; Molecular Probes) at room temperature for 90 min. Then they were counterstained with 2 μg/mL TO-PRO-3 (Molecular Probes) at room temperature for 10 min, and mounted in Gelvatol. A confocal laser scanning microscope (MRC1024; Bio-Rad Laboratories) was used for the morphological analysis.

Quantitative assessment of mitochondrial impairment and cell death

To assess cell viability through mitochondrial impairment, we used the 3-(4,5-dimethyl-thiazol-2yl)-5-(3-carboxymethoxyphenyl)-2-(4-sulfophenyl)-2H-tetrazolium (MTS) assay with CellTiter 96 Aqueous one solution assay (Promega, Madison, WI, USA), as described previously (Takeuchi *et al.* 2002a). At each time point (0, 24 and 48 h) after transfection, MTS assays were carried out in six independent trials. Absorbance at 490 nm was measured in a multiple plate reader as described previously (Ishigaki *et al.* 2002).

Cell death was assessed by the dye exclusion method with propidium iodide (PI; Molecular Probes) as described previously (Takeuchi *et al.* 2002a). At each time point (0, 24 and 48 h) after transfection, cells were incubated with 2 μg/mL PI in DMEM for 15 min at room temperature and mounted in Gelvatol. More than 200 transfected cells in duplicate slides were assessed blindly in three independent trials under a conventional fluorescent microscope. The ratio of dead cells was calculated as a percentage of PI-positive cells among EGFP-positive cells.

Statistical analysis

All results were analyzed by two-way ANOVA with Tukey–Kramer post-hoc test, using Statview software version 5 (SAS Institute Inc., Cary, NC, USA).

Results

Dorfin reduces the levels of total, cytosolic and mitochondrial mutant SOD1

Confocal laser scanning microscopic images revealed that expression of both non-organelle-oriented Cyto-SOD1 plasmid and pcDNA3.1/HisMax-Dorfin was diffusely present in the cells. SOD1-EGFP fusion proteins were co-localized with Xpress-Dorfin fusion proteins (Figs 1a–i), consistent with our previous study (Niwa *et al.* 2002; Takeuchi *et al.* 2002a). In contrast, the expression of mitochondria-oriented Mito-SOD1 plasmid was observed in the mitochondria, as in our previous report (Takeuchi *et al.* 2002a), and was not co-localized with Xpress-Dorfin fusion proteins (Figs 1j–l). Western blots also revealed that Xpress-Dorfin fusion proteins were absent from the mitochondrial fraction (Fig. 1m). At 48 h after transfection, co-expression of Dorfin had reduced the total cell lysate level of SOD1-EGFP fusion proteins expressed by Cyto-G93A or Cyto-G85R by approximately 40%, whereas it did not affect those expressed by Cyto-WT (Fig. 2). In contrast, the amount of SOD1-EGFP fusion proteins expressed by Mito-SOD1 did not show any reduction even with co-expression of Dorfin (Fig. 2). In the cytosolic fraction, co-expression of Dorfin also reduced the level of SOD1-EGFP fusion proteins expressed by Cyto-G93A or Cyto-G85R by approximately 40%, whereas it did not affect those expressed by Cyto-WT (Fig. 3). As we described previously (Takeuchi *et al.* 2002a), cells with Mito-SOD1 showed very small amounts of SOD1-EGFP fusion proteins in the cytosolic fraction (Fig. 3). In the mitochondrial fraction, co-expression of Dorfin also reduced the level of SOD1-EGFP fusion proteins expressed by Cyto-G93A or Cyto-G85R by approximately 50%, whereas it did not affect those expressed by Cyto-WT (Fig. 4). This reduction in mitochondrial SOD1-EGFP was observed from 24 h after transfection, earlier than that of total or cytosolic SOD1-EGFP. In contrast, in the cells with Mito-SOD1, Dorfin did not reduce the amount of mitochondrial SOD1-EGFP fusion proteins (Fig. 4). The above results suggest that the mitochondrial accumulation of mutant SOD1 without organelle-oriented signals might be a result of mutant SOD1 in the cytosol, and we suggest that Dorfin, a cytosolic E3, reduced the accumulation of mutant SOD1 in the mitochondria by enhancing the degradation of mutant SOD1 in the cytosol, not in the mitochondria.

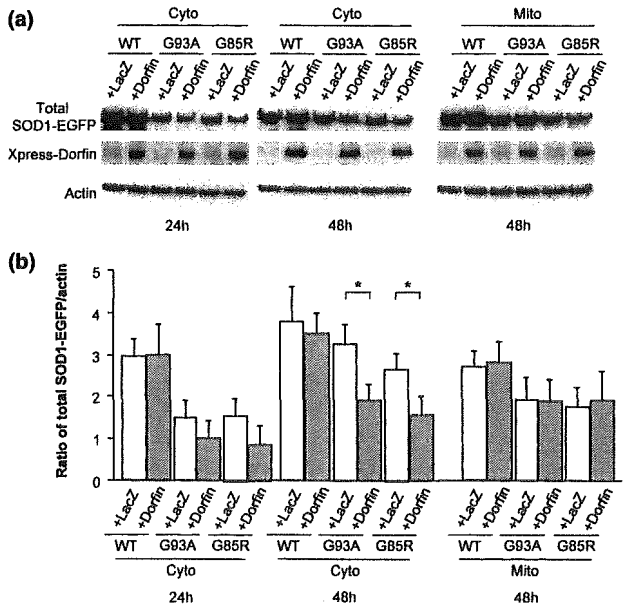

Fig. 2 Level of total SOD1-EGFP fusion protein. (a) Levels of total SOD1-EGFP fusion protein and Xpress-Dorfin fusion protein. (b) Densitometric analysis of total SOD1-EGFP fusion protein expressed as a ratio to actin. Dorfin significantly reduced the level of total SOD1-EGFP fusion protein expressed by Cyto-G93A or Cyto-G85R, whereas it did not reduce that expressed by Mito-SOD1. Values are mean ± SD ($n = 4$). *$p < 0.05$ (two-way ANOVA with Tukey–Kramer post-hoc test).

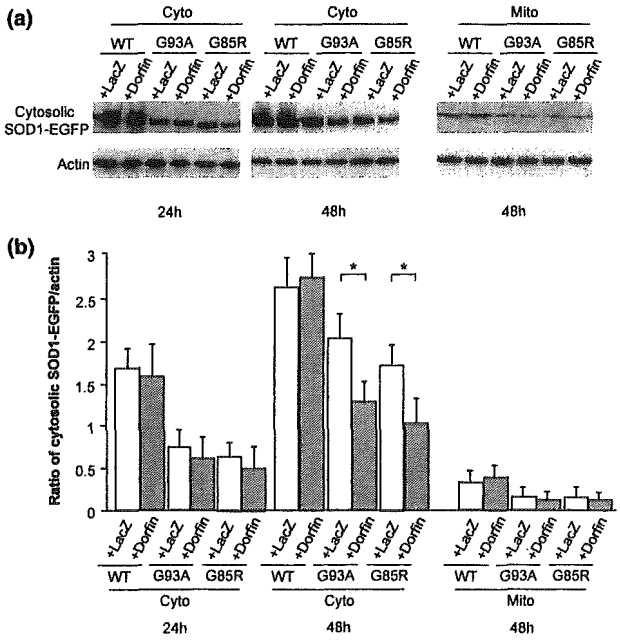

Fig. 3 Level of cytosolic SOD1-EGFP fusion protein. (a) Levels of cytosolic SOD1-EGFP fusion protein. (b) Densitometric analysis of cytosolic SOD1-EGFP fusion protein expressed as a ratio to actin. In the cytosolic fraction, Dorfin significantly reduced the levels of SOD1-EGFP fusion protein expressed by Cyto-G93A or Cyto-G85R. Mito-SOD1 showed very small amounts of SOD1-EGFP fusion proteins in the cytosolic fraction. Values are mean ± SD ($n = 4$). *$p < 0.05$ (two-way ANOVA with Tukey–Kramer post-hoc test).